EES Solar

REVIEW

View Article Online
View Journal | View Issue

Check for updates

Cite this: *EES Sol.*, 2025, **1**, 694

Drift-diffusion modeling of perovskite solar cells: past and future possibilities

Ajay Singh *[a] and Alessio Gagliardi [b]

Approaching 27% power-conversion efficiency and offering solution processability, perovskite solar cells (PSCs) have paved the way for high-efficiency and cost-effective solar cell technologies. Despite huge potential, the commercialization of PSCs is hampered by low stability, *J*–*V* hysteresis, and grain boundary-led performance degradation. Drift-diffusion (DD) modeling has become an indispensable tool for investigating underlying device physics and various dynamical phenomena that are difficult to understand solely using experimental techniques. However, most of the proposed DD models rely on oversimplified assumptions and approximations and therefore do not mimic the actual device while modeling the role of interfaces, doping, mobilities, ionic migration, device architecture, and *J*–*V* hysteresis. Moreover, a significant gap remains in modeling short-term and long-term performance degradation. This review critically examines the evolution of DD modeling in PSCs, highlighting its strengths, limitations, and opportunities for improvement. We discuss strategies to enhance model accuracy by incorporating advanced sub-models for degradation, ionic trapping, mobility, grain boundaries, photon recycling, and quantum effects. We emphasize the incorporation of generation/annihilation of ionic defects and combining time/frequency domain analysis to predict short- and long-term performance degradation. For modeling parameters inaccessible *via* experiments, the possibility of combining DD and Density Functional Theory (DFT) is explored. Furthermore, we present how machine learning models and interfacing experimental data can help speed up and improve the accuracy and reliability of DD models. By identifying current gaps and proposing future directions, this review aims to guide the development of robust, scalable, and physically grounded DD models for PSCs.

Received 25th March 2025
Accepted 15th August 2025

DOI: 10.1039/d5el00040h

rsc.li/EESSolar

Open Access Article. Published on 21 August 2025. Downloaded on 16.02.26 16:33:31.
This article is licensed under a Creative Commons Attribution 3.0 Unported Licence.

Broader context

Perovskite solar cells (PSCs) have rapidly advanced as one of the most promising solar cell technologies due to high efficiency (approaching 27%), low-cost fabrication and tunable optoelectronic properties. Despite huge potential, PSCs' commercialization is hampered by low stability, *J*–*V* hysteresis, and grain boundary-led performance degradation. Drift-diffusion (DD) modeling has emerged as a vital tool for investigating and optimizing PSC performance, offering insights into charge carrier dynamics that are difficult to probe experimentally. This review provides a comprehensive and critical evaluation of DD modeling approaches in PSCs, highlighting their strengths, limitations, and opportunities for improvement. Strategies to refine DD modeling by incorporating advanced sub-models for degradation, ionic trapping, mobility, grain boundaries, photon recycling, and quantum effects are presented. Furthermore, the possibility of combining time/frequency domain analysis, density functional theory and machine learning approaches is presented to improve the accuracy and reliability of DD modeling to predict short- and long-term performance degradations. The broader impact of this work lies in its potential to identify current gaps and propose future directions to guide the development of robust, scalable, and physically grounded DD models for PSCs.

1 Introduction

Hybrid organic–inorganic perovskite solar cells (PSCs) have gained extraordinary attention because of their high power conversion efficiency (PCE) and solution processability. Strong and wide optical absorption, high charge carrier mobilities, long carrier diffusion lengths, and surprisingly low recombination rates in hybrid perovskites have enabled a PCE of 27% in single-junction PSCs and about 35% in silicon/perovskite tandem cells.[1–4] Furthermore, bandgap tunability and low-temperature fabrication techniques make PSCs potential alternatives to develop low-cost solar cells to compete with existing silicon photovoltaic technology.

A typical PSC consists of a transparent conducting oxide (TCO) as one of the electrodes, an electron transport layer (ETL), a perovskite absorber, a hole transport layer (HTL) and a top electrode. TCO is usually deposited on a glass substrate. The

[a]*School of Energy Science and Engineering, Indian Institute of Technology Guwahati, Guwahati, Assam, 781039, India. E-mail: singhajay@iitg.ac.in*

[b]*Chair of Simulation of Nanosystems for Energy Conversion, Department of Electrical Engineering, TUM School of Computation, Information and Technology, Atomistic Modeling Center (AMC), Munich Data Science Institute (MDSI), Technical University of Munich, Hans-Piloty-Straße 1, 85748 Garching, Germany. E-mail: alessio.gagliardi@tum.de*

© 2025 The Author(s). Published by the Royal Society of Chemistry

Open Access Article. Published on 21 August 2025. Downloaded on 16.02.26 16:33:31.
This article is licensed under a Creative Commons Attribution 3.0 Unported Licence.

light enters from the glass/TCO side. Top contact nomenclature comes from the fabrication scheme, as this is the last layer deposited on top of the underlying stack. A metal contact is commonly used as the top contact. Organic and inorganic wide-bandgap semiconducting materials are used as ETLs and HTLs. The absorber material, an organic–inorganic hybrid perovskite, consists of an ABX_3 type crystal structure, where A is an organic cation (such as methylammonium and formamidinium), B is an inorganic cation (such as lead or tin), and X represents the halogen anion (I, Br, and Cl). Fig. 1 shows a typical PSC structure, the perovskite absorber crystal structure and the energy diagram of a PSC. Upon sunlight exposure, electron–hole pairs are generated in the perovskite absorber. Due to the built-in potential arising from different energy levels of the absorber and transport layers, the electrons travel *via* the ETL to the electron collecting electrode. The holes from the absorber valence band travel *via* the HTL to the hole collecting electrode.

Despite high efficiencies demonstrated by PSCs, several long-term and short-term instabilities hinder their commercialization and long-term deployment.[7–9] The photovoltaic performance of PSCs is hampered by grain boundaries (GBs), traps and mobile ionic defects. The role of defects and charge transport in PSCs is a complex phenomenon and not very well understood. The organic–inorganic hybrid nature of the perovskite absorbers introduces complexity in understanding their electronic and optoelectronic behavior. This complexity is further amplified by the interplay of mobile ions, traps, grain boundaries, and introduction of interfaces at the absorber, the charge transport layer (CTL) and electrodes. PSCs exhibit hysteresis in the current–voltage (*J*–*V*) characteristics, which is attributed to a combined effect of traps, grain boundaries and mobile ions, as confirmed by impedance spectroscopy,[10–12] a combination of impedance spectroscopy and deep-level transient spectroscopy,[13] wide-field photoluminescence imaging microscopy[14] and other techniques.[15–17] Ionic defects, grain boundaries, *J*–*V* hysteresis and instabilities in PSCs are regarded to be strongly interlinked; however, their correlation is not very well understood.[11,18–20] Because of mutual dependencies, experimental techniques often fall short in isolating the effects of individual parameters and physical processes such as ionic–electronic interaction, interface recombination, and grain boundary dynamics. Moreover, limitations in measurement techniques may limit the investigation and, hence, the understanding of various fundamental processes at the material and device levels. Simulation models, mainly by decoupling the effects of individual parameters, offer a complementary approach to investigate complex phenomena that would otherwise be difficult to understand using experiments.

Drift-diffusion (DD) is a promising tool to investigate underlying device physics and interface energetics, and to optimize device architecture for obtaining maximum photovoltaic performance of PSCs.[21–24] DD modeling of PSCs has been implemented in several commercial and open course tools, such as SCAPS-1D, Fluxim, OghmaNano, COMSOL, AFORS-HET, TCAD, AMPS-1D, TiberCAD, IonMonger, SIMsalabim and Driftfusion.[25–35] DD models have been employed to optimize material and device parameters, such as conductivity, doping, mobility, thickness and contact work function.[6,24,32,33,36] Apart from device optimization, a significant effort has been dedicated to investigate *J*–*V* hysteresis[17,18,34,37,38] and the role of grain boundaries.[16,27,39,40] However, deeper investigations are required to get a clear picture of the contradictory role of grains.[41–43] The role of ferroelectricity in PSCs has been a topic of debate[44] with several DD models highlighting the importance of

Ajay Singh

Ajay Singh is an Assistant Professor at the Indian Institute of Technology Guwahati (IITG). His research interests are numerical modeling, fabrication and characterization of perovskite solar cells. He also has expertise in modeling device physics in LEDs, nanowires, transistors and quantum structures. After pursuing bachelors and masters at the Indian Institute of Technology Delhi, Singh obtained his doctorate in Engineering from the Technical University of Munich, Germany. Singh has worked as a visiting researcher at the University of Rome Tor Vergata and as a postdoctoral researcher at the University of Luxembourg. Before joining IITG, Singh worked at AVANCIS GmbH, Germany, where his research was focused on developing CIGS/perovskite tandem photovoltaics.

Alessio Gagliardi

Alessio Gagliardi is a professor at the Technical University of Munich, where his research focuses on developing and applying numerical models for simulating nanostructured devices. The development of new models ranges from the nanoscale (Density Functional Theory and Quantum Green Functions) through the mesoscale (Kinetic Monte Carlo) to the macroscopic scale (drift-diffusion and continuum models). The applications of the developed models include new solar cells (based on organic semiconductors and perovskites), electrochemical systems (fuel cells and batteries) and organic semiconductor materials. He is also a developer of TiberCAD and GDFTB software. His latest research is on multiscale modeling for organic semiconductors and using machine/deep learning approaches in materials science. Professor Gagliardi received his doctorate in Physics at the University of Paderborn and pursued postdoctoral research at the Bremen Center for Computing Materials and the University of Rome Tor Vergata (Italy).

Open Access Article. Published on 21 August 2025. Downloaded on 16.02.26 16:33:31.
This article is licensed under a Creative Commons Attribution 3.0 Unported Licence.

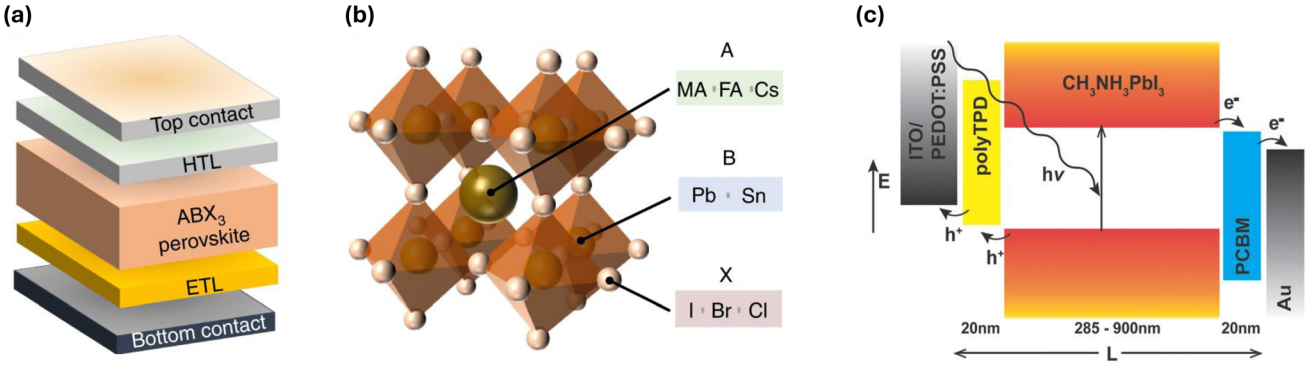

Fig. 1 (a) Typical perovskite solar cell structure. (b) ABX_3 crystal structure of perovskite absorbers. MA, FA and Cs stand for methylammonium, formamidinium, and cesium, respectively. (c) Energy level diagram of a PSC consisting of ITO as TCO, PolyTPD as the HTL, $CH_3NH_3PbI_3$ as the absorber, PCBM as the ETL and gold (Au) as the top contact metal electrode. (a) and (b) are adapted with permission from ref. 5, copyright ©2022, Springer Nature. (c) is adapted with permission from ref. 6, copyright 2017, John Wiley and Sons.

considering the role of ferroelectric domains in perovskite films.[45–47] Along with single-junction PSCs, DD models have been proposed to optimize material and device parameters in perovskite-based tandem solar cells.[24,48–50] Overall, the DD models have made a significant contribution to understanding various aspects of PSCs.

A basic DD model employs solving Poisson's and continuity equations simultaneously for all possible charged species in the system. The continuity equations include generation, recombination, and/or annihilation of charges. By considering only the electrons and holes are generated upon light exposure, a simplified DD model for PSCs can be defined by the following set of equations:[34,37]

$$\begin{cases} \nabla\cdot(\varepsilon\nabla V) = -q(n - p + N_a^- - N_d^+ - N_{ct} + N_{an} + n_t^- - n_t^+) \\ \nabla\cdot j_n = \nabla\cdot\{\mu_n n(\nabla\Phi_n)\} = G - R \\ \nabla\cdot j_p = \nabla\cdot\{\mu_p p(\nabla\Phi_p)\} = -(G - R) \\ \nabla\cdot j_{ct} = \nabla\cdot\left\{\mu_{ct}N_{ct}\left(k_B T\frac{\partial N_{ct}}{\partial x}\right)\right\} = 0 \\ \nabla\cdot j_{an} = \nabla\cdot\left\{\mu_{an}N_{an}\left(k_B T\frac{\partial N_{an}}{\partial x}\right)\right\} = 0 \end{cases} \quad (1)$$

where the first (row) equation represents the Poisson equation consisting of all possible charge densities. Densities of electrons (n), holes (p), ionized donors (N_d^+), ionized acceptors (N_a^-), electron traps (n_t^-) and hole traps (n_t^+) are considered. Mobile ionic defects are well-known in PSCs. For simplicity, two types of ionic defects are considered. Positively charged mobile ions are represented by cations with their density (N_{ct}), and negatively charged mobile ions are represented by anions with their density (N_{an}). The final four equations within the set of eqn (1) are the continuity equations for the electrons, holes, cations, and anions. The negative sign in the hole continuity equation represents the opposite direction of the hole current as compared to the electrons when they both move in the same direction. Any additional charges (if present) must be included in the Poisson equation. Moreover, continuity equations must be defined for additional mobile charges. ε represents the material permittivity, V represents the electrostatic potential, and q represents the elementary charge.

μ_p, μ_n, μ_{ct} and μ_{an} represent the mobility of holes, electrons, cations, and anions, respectively. Φ_n denotes the electrochemical potentials of the electrons and Φ_p denotes the electrochemical potential of holes. All potentials and densities are a function of time and space. Assuming that the anions and cations are neither generated nor recombined, the right-hand sides of the cation and anion continuity equations are set to zero. Further details on the numerical solver can be found in ref. 34, 37, 51 and 52.

In PSCs, electrons and holes can recombine *via* different processes, leading to losses. R represents the net recombination rate governed by the sum of radiative and non-radiative recombination densities. Radiative or direct (bimolecular) recombination is defined as

$$R_{dir} = k_{dir}(np - n_i^2), \quad (2)$$

where k_{dir} is the bimolecular recombination rate coefficient. n_i represents the intrinsic carrier density. To include the effect of trapping of charge carriers by defects and the traps, Shockley–Read–Hall recombination is governed by[53,54]

$$R_{SRH} = \frac{np - n_i^2}{\left(n + N_c\exp\left(\frac{E_t - E_c}{k_B T}\right)\right)\tau_p + \left(p + N_v\exp\left(\frac{E_v - E_t}{k_B T}\right)\right)\tau_n}, \quad (3)$$

where E_t, E_c and E_v represent the trap energy level, the conduction band minimum and the valence band maximum. Note that a trap energy falling within the bandgap is considered. If the trap energy level lies within the conduction band or valence band, the charge carriers get detrapped and can move freely. N_c and N_v are the effective density of states within the conduction and valence bands. τ_p and τ_n are the trapping times of holes and the electrons. The trapping time is defined as a function of the capturing coefficient $C_{n,p}$ and the trap density as follows:

© 2025 The Author(s). Published by the Royal Society of Chemistry

Open Access Article. Published on 21 August 2025. Downloaded on 16.02.26 16:33:31.
This article is licensed under a Creative Commons Attribution 3.0 Unported Licence.

$$\tau_{n,p} = \frac{1}{N_t C_{n,p}}. \quad (4)$$

Higher $C_{n,p}$ and higher trap density (N_t) result in more efficient trapping and hence shorter trapping time $\tau_{n,p}$. In PSCs, recombination in the bulk perovskite films is usually low, which explains the long diffusion lengths of charge carriers and the higher efficiency of PSCs. Therefore, trapping times within the perovskite absorber are considered to be high. On the other hand, due to interface defects, smaller trapping times are considered at the ETL/perovskite and the perovskite/HTL interfaces. Any other recombination process present in the cell should be accounted for in the electron and hole continuity equations.

Upon light exposure, the electron–hole pairs are generated in the perovskite absorber, and the generation rate G is governed by a Lambert–Beer model for absorption:

$$G(x) = \int_{\lambda_{min}}^{\lambda_{max}} \varphi(\lambda)\alpha(\lambda)\exp(-\alpha(\lambda)x)\mathrm{d}\lambda, \quad (5)$$

where $G(x)$ is the generation rate at position x along the film thickness. $\varphi(\lambda)$ denotes the light intensity at given wavelength λ. α represents the absorption coefficient and can be determined experimentally *via* absorption measurements. Alternatively, $\alpha(\lambda)$ as a function of wavelength λ can be extracted by using the imaginary part of the refractive index, κ, defined as[55,56]

$$\alpha(\lambda) = \frac{4\pi\kappa}{\lambda}. \quad (6)$$

κ can be measured by optical measurements such as ellipsometry. The amount of available light within the perovskite absorber is determined by the optical properties of all the layers present in the device stack. The role of various layers can be captured by a transfer matrix method, which is discussed in later sections.

To solve Poisson's equation, two boundary conditions are needed. The common approach is to use Dirichlet conditions (defined-variable value); the potential is fixed at both boundaries at each point at a given time, t. The electrostatic potential boundary conditions can be defined as[39]

$$q(V_l - V(0) + V_{app}) = W_c - W_a \quad (7)$$

where V_{app}, W_a and W_c represent the applied voltage, anode work function and cathode work function, respectively. For simplicity, the potential of one of the contacts can be set to zero as a reference.[34] The charge carrier density boundary conditions at the electrode contacts are given by[39]

$$n, p = N_{cv}\exp(-\psi_{n,p}/V_t) \quad (8)$$

where $\psi_{n,p}$ denotes the offset (in eV) between the anode (cathode) work function and the valence (conduction) band of the perovskite. For the ions, blocking boundary conditions are used as the ions cannot come out of the perovskite layer. The ionic densities as well as the ionic currents are therefore set to zero at both ends of the device.

Most numerical DD models use a finite-element mesh (FEM) to define various layers and their properties in respective regions. During the simulations, a typical approach is to first calculate an equilibrium solution under short-circuit conditions without illumination. Thereafter, the illumination is switched on, and a steady-state solution is obtained. After reaching the steady state, a voltage sweep is applied to obtain the *J–V* characteristics of the device. A simplified one-dimensional model without considering ions and grain boundaries can be used to find steady-state *J–V* characteristics. Such simplified models can be useful for investigating the role of materials and device parameters in optimizing PSCs as presented by Sherkar *et al.*[6] Fig. 2 shows how the *J–V* performance of PSCs can be optimized by varying charge carrier mobility (in the absorber layer), injection barrier (defined by the electrode work functions and the charge transport layer conduction and valence bands), electron trap density, hole trap density, and doping in the HTL.

Approximated steady-state DD models can represent the device performance trends under certain conditions. However, the steady-state models cannot simulate *J–V* curves for different voltage sweep rates, and hence cannot provide information on

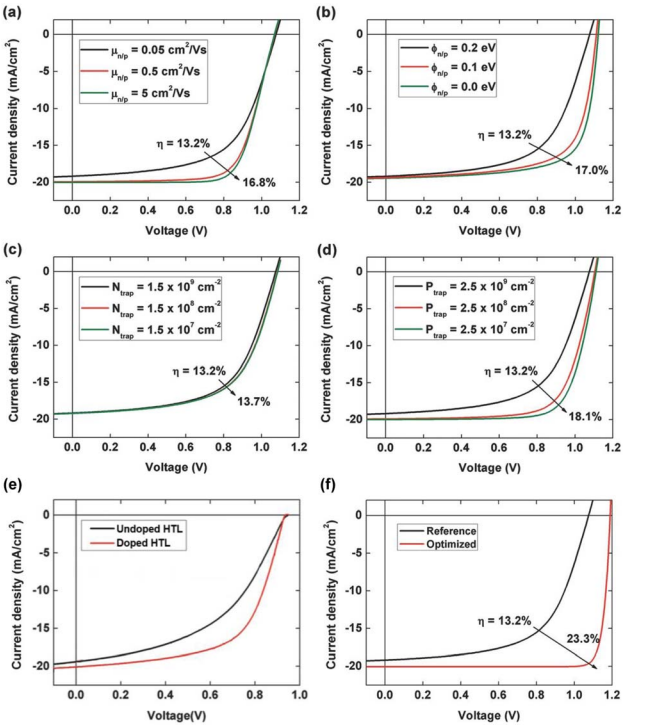

Fig. 2 Simulated *J–V* curves of a perovskite solar cell for different: (a) charge carrier mobilities in the perovskite absorber, (b) injection barriers, (c) electron trap density at the ETL/perovskite interface, and (d) hole trap density at the perovskite/HTL interface. (e) The simulations with and without HTL doping. (f) Optimized device with increased carrier mobilities, reduced energetic barriers and passivated traps. The figure is reproduced with permission from ref. 6 copyright 2017, John Wiley and Sons.

Open Access Article. Published on 21 August 2025. Downloaded on 16.02.26 16:33:31.
This article is licensed under a Creative Commons Attribution 3.0 Unported Licence.

the *J–V* hysteresis. To get information on the hysteresis, a forward bias (low to high voltage) is applied, followed by a reverse bias (high to low voltage). Detailed discussion on *J–V* hysteresis is presented in later sections.

Many DD studies presented in the literature consider various approximations and hence may not represent the real device behavior despite reproducing *J–V* curves as pointed out by Neukom *et al.*[51] Common approximations include geometry considerations, generation and recombination models, the constant temperature approach, the number and parameters of ionic defects, and the role of grain boundaries and interfaces, *etc.* Tessler and Vaynzof have[57] highlighted the importance of including correct models and appropriate parameterization, especially for including the role of ions, dielectric constant, density of states, spatial distribution of recombination losses, *etc.* On the other hand, there has been limited work on modeling of instabilities and hence the device performance in the long run. Minimizing the approximations, better parameterization and incorporation of appropriate submodels are needed to get the real picture of the performance of PSCs. This review critically examines various studies on DD modeling in PSCs to simulate transient and steady-state behavior, interface and grain boundary effects, ionic transport, and long-term stability. A comprehensive review of past studies and their limitations has been presented. Thereafter, we have presented how future studies can adapt emerging strategies to improve the accuracy and predictive power of DD models, such as by implementing refined grain boundary and interface models, machine learning-based acceleration, integration of experimental data, and parameterization with the help of density functional theory calculations. Moreover, we propose on how the inclusion of electronic–ionic interactions and annihilation and creation of ionic defects can help predict short- and long-term performance degradations in PSCs. By thoroughly reviewing current modeling approaches and proposing future pathways for refinement, this review aims to guide the development of robust and physically grounded DD models for PSCs.

2 Geometrical considerations

2.1 Interfaces and grain boundaries

Modeling the interfaces is one of the challenges in simulating PSCs. Most of the studies presented in the literature employ abrupt endings of material on both sides of the interface, which may not be true in a real device. The interfaces between the CTL and the perovskite absorber and between the CTL and electrodes (cathode and anode) play crucial roles in the charge transport and recombination at the respective interfaces. Some studies have defined perovskite/CTL interface regions *via* 1 nm to 2 nm thick layers consisting of traps.[39,51,58] These studies consider the material properties in the interface region same as the perovskite layer. In a real device however, the interface can have a mixture of the perovskite and the particular transport layer. Therefore, a gradual variation of material properties would result in more realistic parameterization for the interface. Some studies have therefore employed a linear variation of material properties at the interfaces between perovskite and the CTL.[37,52,59] The same strategy could be applied to the interfaces between the CTL and the electrodes. However, in-diffusion of: (i) metal into the organic CTL, (ii) ionic defects into the CTL, and (iii) CTL dopants into the interface/bulk absorber can make these interfaces even more complex to model.[60,61] Moreover, a change in built-in potential *via* the formation of self-induced dipoles can change the device performance.[57]

Due to the polycrystalline nature of perovskite films, they consist of several grains oriented in different directions. The boundary between two adjacent grains may consist of dangling bonds, distorted bond angles, and other defects. Traps at the grain boundaries have been regarded as one of the major loss mechanisms in PSC performance.[19,41,42,62] Apart from hosting fixed traps and recombination centers, GBs provide channels for ionic defect migration due to their low activation energies.[41,63,64] Therefore, the GBs play an important role in well-known *J–V* hysteresis in PSCs.[11,41,64,65] A summary of how various studies have modeled grain boundaries in PSCs is presented in Table 1. Olyaeefar *et al.* proposed a classical model combined with a DD model to investigate the impact of grain size and boundary effects in PSCs.[27] The model incorporated the impact of GBs by using equivalent mobility and carrier lifetimes within the perovskite layer itself. Similarly, Iftiquar *et al.* used an AFORS-HET-based one-dimensional DD model to simulate the impact of GBs by incorporating GBs equivalent to the volume defect density within the perovskite layer.[66] Sherkar *et al.* used a one-dimensional DD model to investigate the nature of ionic trap states within grain boundaries using fixed trap densities at points 100 nm apart along the absorber thickness.[39] Nandal *et al.* investigated ion-induced passivation of grain boundaries using a DD model.[67] In the latter, the GBs are defined as 2 nm thick lines along the length and perpendicular to the ETL/perovskite/HTL stack thickness. The GB properties were defined the same as those of perovskite except for a different trap-assisted recombination rate. The study observed that the orientation and location of GBs play an important role in the photovoltaic performance of PSCs. Moreover, GB to GB heterogeneity of adjacent grains can affect the photovoltage in PSCs.[68] Jia *et al.* pointed out the role of GB orientation by investigating the role of residual charges in photovoltaic performance.[69] The study demonstrated that the residual charge exists predominately at the grain boundaries, which are parallel to the device. One of our studies implemented GBs as 1 nm to 2 nm thick regions oriented in different directions in a 2D plane.[16] We observed significant variations in photovoltaic performance with changes in the traps and ionic defect distribution profiles along with GBs. Considering all the aforementioned reports, it is important to correctly capture the size and orientation of the grain boundaries. In a real 3D bulk perovskite film, GBs are oriented in various directions and are distributed randomly. One-dimensional models fail to effectively and accurately mimic GB's orientation and distribution. Going beyond one-dimensional models is a necessity to fairly capture the role of GBs.

Another aspect of GBs is the presence of ordered ferroelectric domains associated with grains oriented in different directions. Rossi *et al.*[46] included the effect of the polarization orientation

© 2025 The Author(s). Published by the Royal Society of Chemistry

Open Access Article. Published on 21 August 2025. Downloaded on 16.02.26 16:33:31.
This article is licensed under a Creative Commons Attribution 3.0 Unported Licence.

Table 1 An overview of grain boundary models used in drift-diffusion simulation of PSCs

Authors, year	GB model	Reference
Olyaeefar *et al.*, 2018	Equivalent mobility and carrier lifetimes within the perovskite layer	27
Iftiquar *et al.*, 2018	Equivalent volume defect density within the perovskite layer	66
Sherkar *et al.*, 2017	Fixed trap densities at certain points along the absorber thickness	39
Chu *et al.*, 2017	A thin slab sandwiched between two adjacent volumes in the 3-dimensional model	70
An *et al.*, 2021	Effective charge carrier recombination rates in the bulk perovskite film	62
Nandal *et al.*, 2019	2 nm lines along with the length and perpendicular to the charge flow in the perovskite layer	67
Singh *et al.*, 2020	Distributed lines in various orientations in a 2-dimensional plane of the perovskite layer	16
You *et al.*, 2021	Two-dimensional grooves in perovskite layers filled with HTL material	71
Kaiser *et al.*, 2022	Distributed points with different energy levels along the absorber thickness	40
Ali Hajjiah, 2025	Horizontal and vertical lines of different thicknesses in a 2-dimensional plane of the perovskite layer	72

pattern in simulating PSCs using a 2-dimensional DD model, as shown in Fig. 3. The study implemented single-grain and multi-grain models using a trap density model associated with GB interfaces. The study highlighted the importance of the inclusion of ferroelectric domain-led polarization to reproduce the experimental *J–V* characteristics. The same group presented another 3-dimensional DD model to investigate the role of ferroelectricity in PSCs.[47] Importantly, such 2-dimensional and 3-dimensional DD models can be extended to investigate the combined role of grain boundaries (such as defect states and ionic migration) and ferroelectricity.

Overall, accurate representation of grain boundaries, interfacial energetics and local variations is imperative for enhancing the predictive fidelity of DD simulations, as these regions critically influence charge transport, recombination dynamics, and overall device performance in PSCs.

2.2 Mesoporous *versus* planar structure

Mesoporous scaffold in PSCs offers higher surface area to form contact between the perovskite and charge transport layer, thereby resulting in improved charge extraction.[73,74] A one-dimensional FEM cannot define mesoporous layers and therefore higher-dimensional geometries are desired. Commercial 3D simulation packages combining finite-difference time-domain and FEM have been used to simulate PSCs.[28,75,76] However, most of these studies use planar architectures and make several approximations for the number of charged species and their interactions. In one of our studies, we presented a 2D mesh-based DD model to investigate the role of perovskite infiltration into mesoporous TiO_2.[29] The study gives a good approximation of the role of pore-filling and the interface defects, in agreement with the experimental findings, as shown in Fig. 4. To get a complete picture however, a 3D mesoporous FEM is desired.

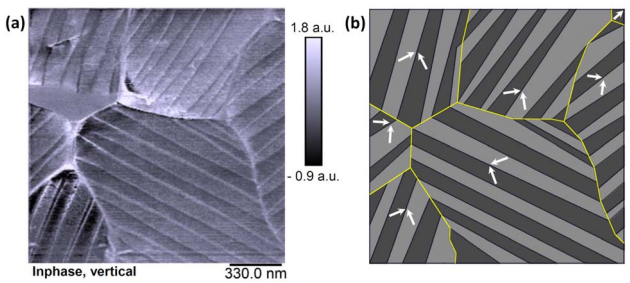

Fig. 3 (a) Piezo-response force micrographs and (b) the anticipated ferroelectric domain polarization used in the DD model as a representative of the multi-grain surface section. Reproduced from ref. 46, copyright (2018), with permission from Elsevier.

2.3 Charge carrier generation profile and local variations in the bandgap and defects

The charge carrier generation is determined by the amount of available light and the absorption coefficient of the absorber layer. Several studies consider constant or exponential decay charge carrier generation profiles obtained using the Lambert–Beer model for absorption while omitting the role of transport layers and contacts.[17,38,58,77–79] However, a real device undergoes reflection and parasitic absorption losses in the CTL and electrodes. The reflections and interface patterns from various layers can significantly modify the optical profile and hence the charge carrier generation in the absorber layer. The optical profile is governed by the thickness and optical constants (refractive index, n_r, and extinction coefficient, k) of all the layers stacked together. Several studies simulate the role of metal contacts as a fixed workfunction.[17,78–81] A PSC's back contact determines if the unabsorbed light will be transmitted or reflected back to the absorber. A reflection from a metal back contact permits more absorption in the absorber layer. This phenomenon can explain why opaque metal contact may result in higher current densities in comparison to semitransparent back contact while keeping the remaining layers unchanged.[29] To directly assess the PSC's performance, a correct optical profile must be obtained. The transfer matrix method combined with absorption models is a method that properly accounts for the optical role of the various layers and accurately calculates charge carrier generation rates.[6,59,82–85]

During the cell operation, the charge carriers undergo trapping and/or recombination, which strongly depends on the available charge carrier density. At a given point, a higher charge carrier generation implies a higher recombination probability. The traps and recombination centers can be non-uniformly distributed throughout the device stack. The distribution of recombination centers combined with different

Open Access Article. Published on 21 August 2025. Downloaded on 16.02.26 16:33:31.
This article is licensed under a Creative Commons Attribution 3.0 Unported Licence.

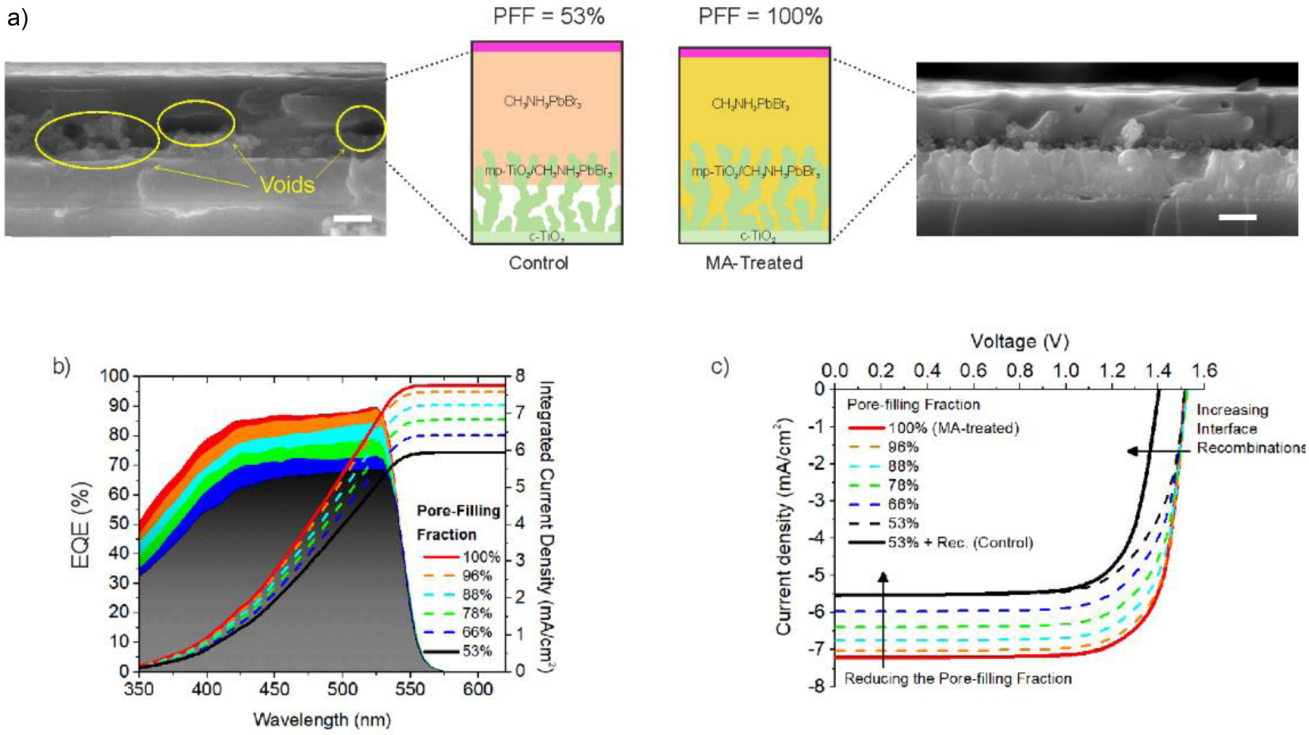

Fig. 4 2-Dimensional DD model corroborating the experimental findings on pore-filling of perovskite into mesoporous TiO_2. (a) SEM images and DD model input geometry for the pore filling factor (PFF). (b) Calculated external quantum efficiency (EQE) and integrated current density. (c) Calculated J–V characteristics with different pore filling and interface trap densities. The traps are considered at the mesoporous TiO_2/perovskite interface. The cell stack consists of FTO/compact-TiO_2/mesoporous-TiO_2/$CH_3NH_3PbBr_3$/PTAA/gold. Reproduced with permission from ref. 29, copyright 2021, John Wiley and Sons.

carrier distributions can affect the photovoltaic performance.[86] If the regions with higher defects (such as interface traps) and high charge carrier generation coexist at the same point, there will be more trapping/recombination, and *vice versa*. Fig. 5 elaborates on the scenario by considering simplified charge carrier generation profiles and recombination centers.

For simplicity, the effects of ETL, HTL and contact layers are ignored. Generation profile G_1 (G_2) is obtained if the cell is illuminated from the ETL (HTL) side. Values for the perovskite layer thickness and charge carrier generation rate are taken as typical values for PSCs based on the literature. As an example, in the case of G_1 (the maximum value chosen based on ref. 6, 16 and 52), electron traps near the ETL/perovskite interface will experience 1×10^{22} cm^{-3} electrons. If the light is incident from the HTL side, the same electron traps will experience 1×10^{20} cm^{-3} electrons for a possible trapping/recombination. Therefore, the recombination losses will be higher in the case of illumination from the ETL side. Similarly, hole traps will affect the device's performance based on their position and the illumination side in the cell. The charge carrier profile and hence the trapping/recombination will be modified by the 'light reflection and interference patterns' while considering CTL and the contacts. Our recent study explains why illuminating from the TiO_2 (ETL) side results in a different loss mechanism than illuminating from the opposite side.[87] This can also explain why p-i-n and n-i-p structures have different charge transport mechanisms given the same absorber quality.[88,89]

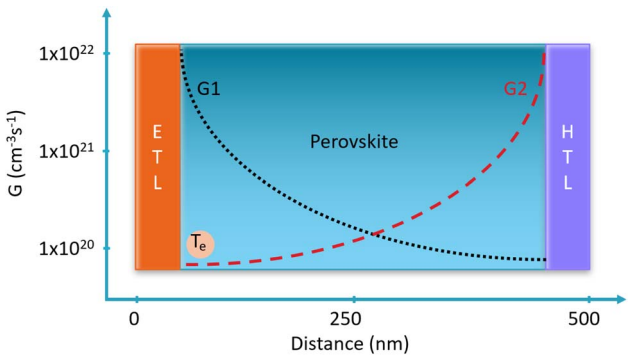

Fig. 5 Charge carrier generation profiles and electron traps in a perovskite solar cell. T_e represents an electron trap near the perovskite/ETL interface. G_1 and G_2 represent generation profiles upon light irradiance from the ETL and HTL sides, respectively.

Furthermore, local variations in bandgap can modify light absorption and hence charge carrier generation and their recombination profiles and ultimately the photovoltaic performance.[90,91] Also, a difference in the bulk and surface work functions can modify the charge extraction and hence the photovoltaic performance. Canil *et al.* observed a significant change in the photovoltaic performance upon tuning the surface work function of the perovskite layer.[58] Overall,

© 2025 The Author(s). Published by the Royal Society of Chemistry

Open Access Article. Published on 21 August 2025. Downloaded on 16.02.26 16:33:31.
This article is licensed under a Creative Commons Attribution 3.0 Unported Licence.

considering appropriate optical models and the right spatial distribution of bandgap, traps and other properties are needed to obtain accurate and reliable results of a DD model.

2.4 Barrier layers and tunnelling effect

Various architectures employ thin barrier layers to block ionic transport to the CTL. Surface passivation using 2D MXenes, 2D perovskites, and dipole interlayers are well-known practices in high-efficiency state-of-the-art PSCs.[90,92,93] On the other hand, self-assembled monolayers as hole transport layers have gained great attention in recent years.[94] Most existing DD studies consider the passivating layer properties similar to the bulk perovskite layer itself. Our simulations for the effect of 'interface work function tuning' found the variation in photovoltaic performance correlating to the experimental values.[58] In the study, we approximated the functionalized surface as a 2 nm layer similar to the bulk perovskite except for a different work function. For simplicity, we ignored the effect of quantum transport and considered abrupt junctions between various layers. To fairly include the effect of 2D passivating layers and self-assembled monolayers, quantum models should be adapted to account for the energy-level modification and tunnelling-dependent charge transport. For example, various p-i-n devices employ a thin BCP (bathocuproine) layer, which in principle can act as a tunnelling layer for electrons and a blocking layer for holes.[95,96] Depending on the thickness, the BCP layer leads to an improved fill factor or an "S" shape in the *J–V* characteristics. Considering just the blocking nature of this layer may result in misleading results.[79,97] In a thin layer, Fermi-level pinning moderates the charge transport despite huge energy barriers presented by the valence and conduction band energies. Tian *et al.* presented a combined drift-diffusion and quantum transport model for an n-type TOPCon silicon solar cell.[98] The study found significant differences in the photovoltaic performance with and without considering the quantum transports. Similarly, to draw a complete picture of charge transport in PSCs *via* various layers and interfaces, quantum models in combination with the DD model are needed.

3 Ionic transport and *J–V* hysteresis

Weak metal-halide bonds within the halide perovskites (ABX_3) form a soft lattice that is prone to dynamic structural disorders and defects in the crystal.[9,99–101] The softness of the crystal makes halide perovskites unstable against temperature variations.[101] Charged ionic defects such as interstitials and vacancies of halide anions, metal cations and organic cations can freely move within the perovskite absorber.[13,99,102–104] Ionic defect migration has been considered to be the main reason behind *J–V* hysteresis (forward bias and reverse bias scans do not follow each other) in PSCs.[11,15,17,37,105] Ions can passivate GBs depending upon the polarity of ions and the location of GBs,[67] and modulate the photovoltaic performance.[106,107] Moreover, chemical reactions driven by the ionic defects (such as iodine ions) can lead to non-reversible degradation of the perovskite absorber.[107] Modeling the mobile ions' movement is one of the most complex processes to implement within DD models. This is mainly because of the lack of experimental values for parameters such as the types of ionic defects, their densities, distribution profiles, mobilities, diffusion coefficients, and preferred migration channels. Upon illumination, the photo-enhanced ion conductivity makes it even more complex to determine adequate parameters for ions.[108]

Most of the DD studies consider one positive and one negative ionic species to investigate the impact of ions on photovoltaic performance.[18,38,51,52,109] In a real device however, different ionic defects can result in more than two species of mobile ions moving with different properties including densities, mobilities, and associated energy levels. Considering more than two ionic species can pinpoint which species are responsible for particular characteristics. For example, certain mobile ions with a given density and mobility may not result in *J–V* hysteresis, while the others can contribute to the same.

Not only are the types and densities of ionic defects under debate, but their distribution and migration channels are as well. The densities and distribution of ionic defects play a crucial role in determining steady-state photovoltaic performance.[16,67] Some studies have suggested that the ionic defects move through the grain boundaries due to the lower activation energies at the GBs than the bulk of the grains.[63–65] One-dimensional DD models fail to capture simultaneously the GBs and the ionic movements *via* them, and therefore several approximations are considered. Table 2 summarizes some of the key DD studies that have investigated the impact of various ionic defects in PSCs, considering their different types, densities, and distribution profiles. Sherkar *et al.* considered fixed trap density to mimic ionic defects in their 1D simulations to investigate the nature of ionic trap states within grain boundaries.[39] Gagliardi *et al.* defined fixed electrostatic potential within the mesoporous TiO_2 layer to mimic ionic distribution.[110] Canil *et al.* modeled steady-state photovoltaic performance by considering ions distributed within 2 nm interface layers between the perovskite and CTLs.[58] Some studies have considered the uniform ionic distribution within the perovskite layer.[37,38,51,59] Overall, the combined role of ionic defects and grain boundaries in photovoltaic performance is not very well understood. To get the real picture, a two- or three-dimensional (both transient and steady-state) model consisting of GBs and multiple ionic species is desired.

Another important aspect to consider while modeling the impact of ions is their interactions with electrons and holes. Le Corre[36] modeled transient behavior by neglecting the effect of ions and SRH recombination, assuming that the ions do not move significantly at the microsecond timescale. In the model, including traps and SRH recombination or fixed ions resulted in identical outcomes similar to the case when only bimolecular recombination was considered. To note that the scenario when only bimolecular recombination is present is similar to the open-circuit condition (cell delivers no power). In a real solar cell, it is (almost) impossible to avoid non-radiative recombination. Neukom *et al.* modeled the steady-state and transient behavior while considering no interaction of ions with electrons, holes and traps.[51] Calado *et al.* implemented a one-

Open Access Article. Published on 21 August 2025. Downloaded on 16.02.26 16:33:31.
This article is licensed under a Creative Commons Attribution 3.0 Unported Licence.

Table 2 Various drift-diffusion modeling studies on investigating *J–V* hysteresis and the role of ionic defects in PSCs

Authors, year	Ionic density	Ionic distribution	Remarks and findings	Reference
Reenen *et al.*, 2015	1×10^{15} cm^{-3} to 1×10^{19} cm^{-3}	Free to move within the perovskite layer	*J–V* hysteresis is a combined effect of mobile ions and traps. No hysteresis without traps	111
Richardson *et al.*, 2016	1×10^{17} and 1.6×10^{19} cm^{-3}	Free to move within the perovskite layer	Slow moving ions lead to *J–V* hysteresis	17
Calado *et al.*, 2016	1×10^{15} cm^{-3}	Distributed within the perovskite layer	Combination of mobile ions and recombination centres leads to *J–V* hysteresis	52
Sherkar *et al.*, 2017	1×10^{15} cm^{-3}	Distributed within the perovskite layer and at the GBs	Ions can fill grain boundary traps and change the *J–V* hysteresis profile	39
Gagliardi *et al.*, 2017	1×10^{16} cm^{-3} to 1×10^{19} cm^{-3}	Distributed at the perovskite/TiO_2 mesoporous interface	Increased surface area dilutes the effect of ion accumulation	110
Domanski *et al.*, 2017	1×10^{17} cm^{-3}	Distributed within the perovskite layer	Trapping of electrons at mobile cations may lead to reversible performance losses	112
Canil *et al.*, 2021	1×10^{17} cm^{-3}	Fixed charge density at perovskite interfaces	Ion accumulation at the interface affects the steady-state performance	58
Neukom *et al.*, 2019	5×10^{17} cm^{-3}	Distributed within the perovskite layer	Charge injection is affected by ion accumulation at perovskite interfaces	51
Nandal *et al.*, 2019	1×10^{17} cm^{-3} and 1×10^{18} cm^{-3}	Distributed at the grain boundaries	Ions can passivate the effect of grain boundary losses	67
Singh *et al.*, 2020	1×10^{16} cm^{-3} to 1×10^{19} cm^{-3}	Fixed in the bulk, at the grain boundaries and at the perovskite interfaces	Steady-state performance changes with ionic distribution	16
Singh *et al.*, 2021	1×10^{18} cm^{-3}	Free to move within the perovskite layer	Cation-assisted recombination enhances *J–V* hysteresis to experimentally observed values. Nominal *J–V* hysteresis without cation-assisted recombination	37
Calado *et al.*, 2021	0 cm^{-3} to 1×10^{19} cm^{-3}	Distributed within the perovskite layer	Ionic redistribution screens the electric field and determines the steady-state performance	59
Zhou *et al.*, 2021	5×10^{17} cm^{-3}	Distributed within the perovskite layer	Dielectric constant of charge transport layers affects the hysteresis	38
Minbashi *et al.*, 2022	9×10^{16} cm^{-3}	Distributed within the perovskite layer	Inverted hysteresis is obtained when ions accumulate at the perovskite boundaries	109
Almora *et al.*, 2024	1×10^{15} cm^{-3} to 1×10^{18} cm^{-3}	Distributed within the perovskite layer	Different recombination mechanisms are present at different ionic densities	113
Wang *et al.*, 2024	1×10^{16} cm^{-3} to 1×10^{18} cm^{-3}	Distributed within the perovskite layer	*J–V* hysteresis is linked to device degradation	18

dimensional time-dependent DD model to study the role of ionic migration in *J–V* hysteresis.[52,59] In their model, ions were considered to only screen the built-in potential, while trapping of charge carriers was neglected. However, several studies have pointed out the trapping nature of accumulated iodine vacancies at GBs and interfaces.[114–116] Trapping by ionic defects might be one of the essential factors in *J–V* hysteresis, as modeling without traps can result in hysteresis-free *J–V* profiles.[6,37,52,111] In a joint experimental and theoretical study by Domanski *et al.*, the DD model included the recombination of electrons at mobile anions to investigate the transient behavior of photocurrent.[112] This study was the first (to our knowledge) one to analyze electrons' recombination at anions using a simplified bimolecular recombination model. Our previous study included electron trapping (and electron–hole recombination) at the mobile cation sites.[37] The study found that "ions-led built-in

© 2025 The Author(s). Published by the Royal Society of Chemistry

Open Access Article. Published on 21 August 2025. Downloaded on 16.02.26 16:33:31.
This article is licensed under a Creative Commons Attribution 3.0 Unported Licence.

field screening only" leads to very low hysteresis compared to the experimentally observed values. Adding cation-mediated electron–hole recombination results in hysteresis values similar to those experimentally observed. To our knowledge, trapping phenomena caused by the anions have not yet been studied. Fig. 6 shows calculated *J–V* profiles for various cases, *i.e.*, with and without ions, with ions and traps, and with ions, traps and cation-mediated recombination. Considering various possible trapping and recombination processes, it is still difficult to pinpoint the exact mechanism leading to the *J–V* hysteresis. Possibly, multiple phenomena contribute to the effect, and it is hard to experimentally measure independent contributions of various processes. DD models can help decouple the contributions of various phenomena responsible for the hysteresis. However, the material and device parameterization is not coherent throughout the proposed studies. Therefore, appropriate parameterization on types and the number (could be more than two) of ionic species, and their energy levels, densities, mobilities, migration channels and interactions with charge carriers is necessary to draw a fair conclusion on the complex role of ionic defects.

4 Mobility models

Several DD models employ constant mobility models in the perovskite absorber and CTL. In hybrid perovskite films, charge carriers and ionic defect mobilities depend on various factors, such as film stoichiometry, self-doping, energetic disorders, grain size, and ionic defect scatterings.[117–120] Moreover, during the operating conditions, temperature variations, degradation and other factors may change the charge carrier and ionic defect mobilities. More studies are needed to investigate the behavior of charge carriers and ionic mobilities within the perovskite absorbers. On the other hand, charge carrier mobilities in transport layers depend on temperature, doping and electric field.[121] Therefore, modeling PSCs with constant mobility models may result in misinterpreting the calculated data. The inclusion of factors such as doping and temperature dependence is very important while modeling PSCs.

4.1 Temperature-dependent mobility

In a semiconductor crystal, lattice/phonon scattering and ionized impurity scattering affect the charge carrier mobilities.[122,123] Both the lattice scattering and ionized impurity scattering depend on the operating temperature. A generalized temperature-dependent mobility can be defined as

$$\mu_T = \mu_0 \left(\frac{T}{T_0}\right)^m, \tag{9}$$

where $T = 300$ K is the reference temperature. m is a constant governed by the scattering mechanisms in the material. The inelastic scattering of optical phonons results in a power law of $\mu \propto T^{-1/2}$, and the elastic scattering of acoustic phonons results in a power law of $\mu \propto T^{-3/2}$. Charge carrier scattering of ionic defects and impurities results in a power law of $\mu \propto T^{+3/2}$. In a hybrid perovskite film, mobilities can vary with film stoichiometry, self-doping, energetic disorder, grain size, and ionic defect scatterings.[117–120] Therefore, a mixture of various effects can lead to a different power law dependence. Biewald *et al.*[124] obtained a power law dependence of $\mu \propto T^m$ with $m = -(1.8 \pm 0.1)$ for MAPI perovskite. A theoretical study by Mayers *et al.* proposed a power law dependence of $\mu \propto T^{-2.11}$.[125] Savenije *et al.* proposed band-like dependence of mobility with $\mu \propto T^{-1.6}$.[126] Moreover, hybrid perovskite may undergo a phase change and the charge carrier mobility can differ in different crystalline phases.[124]

4.2 Doping dependent mobility

In PSCs, CTLs are doped to efficiently transfer the charges from the absorber to the electrodes. Both organic and inorganic CTLs have been used in perovskite solar cells.[127,128] In widely used organic CTLs (such as Spiro-OMeTAD, Spiro-TTP, PolyTPD, PEDOT:PSS, C_{60}, BCP, PCBM, PTAA, *etc.*), the charge

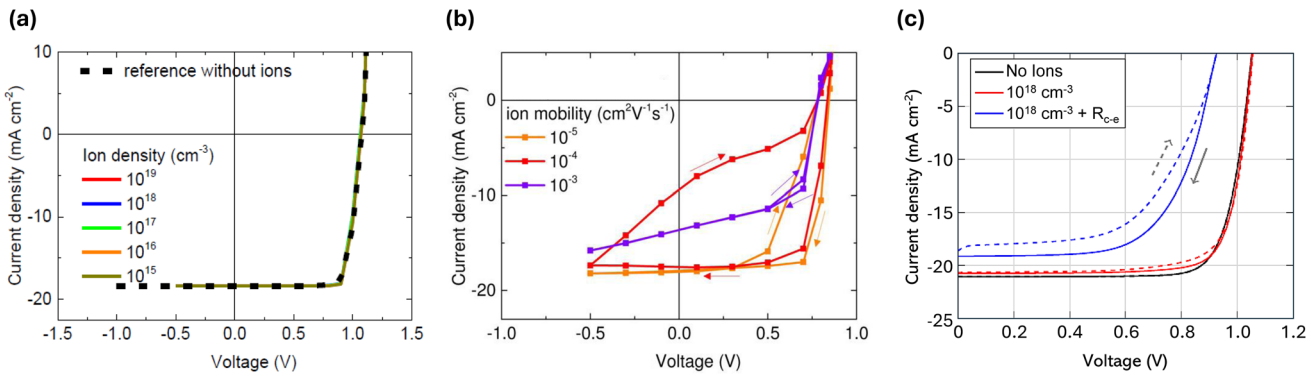

Fig. 6 Calculated *JV* characteristics for PSCs resembling FTO/TiO_2/$CH_3NH_3PbI_3$/Spiro-OMeTAD/gold devices: (a) comprising ions and no traps, (b) comprising ions and traps, and (c) comprising no ions, comprising ions and cation-assisted recombination. Red and blue curves in (c) correspond to an ion density of 10^{18} cm^{-3}. $R_{c\text{-}e}$ represents the presence of cation-assisted recombination. Both the anion and cation densities were kept the same to maintain charge neutrality. The arrows denote the sweep direction. Subfigures (a) and (b) have been adapted with permission from ref. 111, copyright 2015 American Chemical Society. Subfigure (c) has been adapted with permission from ref. 37, copyright 2021, Elsevier B.V.

© 2025 The Author(s). Published by the Royal Society of Chemistry

Open Access Article. Published on 21 August 2025. Downloaded on 16.02.26 16:33:31.
This article is licensed under a Creative Commons Attribution 3.0 Unported Licence.

carrier mobility is a complex function of host–dopant interactions. Several groups have investigated doping-dependent mobility in organic semiconductors.[129–132] Arkhipov *et al.* presented an analytical model to calculate charge carrier mobility in weakly and heavily doped organic semiconductors.[133,134] Koopmans and coworkers studied the electrical conductivity of fullerene derivatives.[135] Doping-dependent charge carrier mobilities for inorganic semiconductors can be found using empirical models similar to the ones proposed for silicon.[136,137] Along with the CTL, intentional or self-doping in the hybrid perovskites can change charge carrier mobilities in the absorber layer.[117,119,138]

Overall, to fairly capture the role of varying mobilities, appropriate temperature- and doping-dependent mobility models should be employed.

5 Stability

5.1 Ionic defect and grain boundary driven instabilities

One of the major concerns hampering the commercialization of PSCs is their poor stability. Intrinsic factors such as ionic defects, surface and interface defects, grain boundaries, nanoscale phase impurities, and inhomogeneities have been reported to affect the short-term and long-term stabilities of PSCs.[91,139–141] Moreover, extrinsic factors such as exposure to light, temperature, and moisture affect the operational stability of PSCs. Nandal and Nair presented a modeling of ionic-migration-induced performance degradation in PSCs.[142] The origin of ionic defects can be both the intrinsic and extrinsic factors involving chemical processes leading to the creation and annihilation of ionic/neutral species.[143–145] Bitton and Tessler combined the DD model with iodine chemistry to investigate the annihilation of electrons and holes.[107] The study points out that certain chemical reactions can lead to mobile ionic defects and, hence, deterioration of the photovoltaic performance during the cell operation. The study considered only radiative recombination losses and the SRH recombination was ignored. Theoretically, a negative ionic defect can capture a hole to become electrically neutral or can remain negatively charged *via* facilitating electron–hole recombination. Similarly, a positive ionic defect may facilitate electron–hole recombination by capturing an electron. In the case of cation-assisted and anion-assisted recombination of electrons and holes, the electron and hole continuity equations should be updated with additional recombination processes. The updated electron and hole continuity equation can be written as:

$$\begin{cases} \nabla\cdot\{\mu_n n(\nabla\Phi_n)\} = G - R - R_{ct} - R_{an} \\ \nabla\cdot\{\mu_p p(\nabla\Phi_p)\} = R + R_{ct} + R_{an} - G \end{cases} \quad (10)$$

where R_{ct} and R_{an} represent the net electron–hole recombination rates led by cations and anions, respectively. The ion-assisted recombination rates can be modeled as defined in ref. 37.

The creation and annihilation of new charged species will lead to disruption of the perovskite absorber crystal and hence a drop in photovoltaic performance. The DD model can help predict photovoltaic performance losses by accounting for the newly formed charged species. If new charged species are created and annihilated (without involving free electrons and holes), additional continuity equations need to be defined for each charged species. The continuity equations for the newly created/generated cations and anions in eqn (1) can be defined as

$$\begin{cases} \nabla\cdot\left\{\mu_{ct,new}N_{ct,new}\left(k_BT\dfrac{\partial N_{ct,new}}{\partial x}\right)\right\} = G_{ct,new} - R_{ct,new} \\ \nabla\cdot\left\{\mu_{an,new}N_{an,new}\left(k_BT\dfrac{\partial N_{an,new}}{\partial x}\right)\right\} = R_{an,new} - G_{an,new} \end{cases} \quad (11)$$

where $G_{ct,new}$, $R_{ct,new}$, $G_{an,new}$ and $R_{an,new}$ represent the rates of creation of new cations, annihilation of new cations, creation of new anions, and annihilation of new anions, respectively. Note that the continuity equations for new charged species (ct,new and an,new) are in addition to the existing continuity equations as defined in eqn (1) (for electrons, holes, existing cations and existing anions). At the same time, the Poisson equation (defined in eqn (1)) should be modified by including new charged species as follows:

$$\begin{cases} \nabla\cdot(\varepsilon\nabla\Psi) = \\ -q(n - p + N_a^- - N_d^+ - N_{ct} + N_{an} + n_t^- - n_t^+ - N_{ct,new} + N_{an,new}) \end{cases} \quad (12)$$

Overall, including the creation/annihilation of electrically charged and neutral species and the ionic-assisted recombination processes can help predict instantaneous as well as long-term fluctuations in photovoltaic performance.

Many DD models presented in the literature ignore the GB-assisted degradation in PSCs. By visualizing the spatial evolution of local photoconductivity, Chu and co-workers reported that the degradation process is triggered by the disintegration of grains rather than 'nucleation and propagation' from visible grain boundaries.[70] This leads to the evolution of the shape and size of GBs over time. This GB-led change in the distribution of defects and ionic species will change photovoltaic performance.[16] Moreover, spontaneous grain coalescence in the dark can enable the reduction of grain GB-led photovoltaic losses.[65] By accounting for grain boundaries and evolved concentrations of static and mobile defects at GBs, DD models can help to

© 2025 The Author(s). Published by the Royal Society of Chemistry

Open Access Article. Published on 21 August 2025. Downloaded on 16.02.26 16:33:31.
This article is licensed under a Creative Commons Attribution 3.0 Unported Licence.

investigate the role of GBs' evolution in the short-term and long-term performance of PSCs.

5.2 Thermal instabilities

Hybrid perovskites are shown to degrade under high temperatures *via* chemical reactions. The temperature influences the rate of chemical reactions and, hence, the rate of annihilation and creation of ionic defects. Variations in the 'ionic defect's density and distribution' change the ionic–electronic interactions and built-in field screening, and hence, the solutions to the Poisson and continuity equations. Moreover, the charge carrier (electronic–electronic) trapping and recombination times depend on temperature, defined as[146]

$$\tau_n = \tau_n^0 \left(\frac{T}{T_0}\right)^{\alpha_n} e^{\beta\left(\frac{T}{T_0}-1\right)}. \quad (13)$$

Thermal variations also influence the charge carrier and ionic defect mobilities as discussed in previous sections. Furthermore, a temperature variation can change the bandgap of a semiconductor, especially the absorber layer. The temperature-dependent material bandgap is defined as follows:[147]

$$E_g(T) = E_g(0) - \frac{\alpha_1 T^2}{T + \beta_1} \quad (14)$$

where $E_g(0)$, α_1 and β_1 are material constants. The change in bandgap (conduction and valence band energies) leads to a change in equilibrium charge carrier concentrations, defined as

$$n = N_c \exp\left(\frac{E_{fn} - E_c}{k_B T}\right) \text{ and } p = N_v \exp\left(\frac{-E_v + E_{fp}}{k_B T}\right), \quad (15)$$

where N_c and N_v are the temperature-dependent effective densities of states of the conduction and the valence bands, respectively, defined as[123]

$$N_c = 2\left(\frac{2\pi m_e^* k_B T}{h^2}\right)^{\frac{3}{2}} \text{ and } N_v = 2\left(\frac{2\pi m_h^* k_B T}{h^2}\right)^{\frac{3}{2}}. \quad (16)$$

Similarly, the position of the Fermi level in doped semiconductors (*i.e.*, the electron and hole transport layers) strongly depends on the operating temperature.[123] Therefore, during the cell operation, the temperature-dependent charge carrier concentrations should be updated in the continuity and Poisson equations. Along with carrier concentrations, the temperature change can induce changes in charge carrier and ionic mobilities as explained in an earlier section. Overall, the temperature variation can change the concentrations, mobilities, and interaction patterns of various charged species within a PSC. To accurately consider the temperature dependence (especially while modeling the time-dependent performance evolution), the ionic defect creation and annihilation rates, carrier densities, mobilities, and their interaction should be implemented in appropriate equations.

6 Further improvements

6.1 Inclusion of optical models and photon recycling

Optical modeling within DD governs the light absorption and the spatial distribution of photogenerated carriers, which directly influences recombination dynamics and device efficiency. The transfer matrix method in conjunction with the Lambert Beers model nicely defines the optical generation rate in a homogeneous absorber with no bandgap variations. Heterointerface-driven instabilities can however lead to bandgap variations and hence change in the light absorption (hence the charge carrier generation) profile locally.[90,91] Optical models accounting for local variation are desired in such cases. In high-efficiency devices where the defect-assisted non-radiative losses are nominal, radiative losses become the dominant loss mechanism. When the cell is producing non-zero output power, radiative recombination of electrons and holes results in photons that can be absorbed in different regions of the absorber layer. This phenomenon is commonly known as photon recycling. In the case of bandgap inhomogeneities and graded bandgap structures, photon recycling becomes even more prominent as the photon emitted by the high bandgap region can be absorbed by a low bandgap region. Incorporating photon recycling models within the DD can help improve the accuracy of the calculated data similar to the ones reported in GaAs solar cells[148] and all-perovskite tandem solar cells.[149] Zeder *et al.* have demonstrated a coupled photon-recycling DD model for PSCs.[150] The model incorporated Green's function formalism with a charge-carrier DD model to account for reabsorption of internally emitted light. Improvements in both V_{oc} and efficiency were observed upon inclusion of photon recycling. Brenes *et al.* presented a combined experimental and detailed balanced model to calculate the effect of photon recycling on the *J–V* performance of PSCs.[151] Upon accounting for the effect of light scattering in a photon recycling model, the study found an increase (77 mV) in V_{oc}. The study, however, does not account for local variations in bandgap and non-radiative near-field coupling to the nearby perovskite. However, both the studies point out the underestimation of simulated photovoltaic performance of PSCs while ignoring the photon recycling. The inclusion of bandgap inhomogeneities and photon recycling in DD models remains largely unexplored. Therefore, studies integrating wavelength (bandgap)-resolved optical models and photon recycling mechanisms into DD frameworks are critical for accurately capturing the local and global carrier generation and recombination in PSCs.

6.2 Time/frequency dependence

Steady-state DD modeling cannot capture the effect of several kinetic phenomena occurring in PSCs at short time scales, especially those linked to ionic defects. Since the ions remain within the perovskite layer itself and cannot be transported to the external contacts, accurately capturing their interactions becomes very important. To capture such phenomena, time- and frequency-domain analyses are needed for the stacks with and without charge transport layers. Incorporating light

Open Access Article. Published on 21 August 2025. Downloaded on 16.02.26 16:33:31.
This article is licensed under a Creative Commons Attribution 3.0 Unported Licence.

intensity-dependent open-circuit voltage and photocurrent, capacitance–voltage, transient photocurrent and voltage-step responses provides deeper insights into various phenomena not captured by simple DD models.[21] Bou *et al.*[152] have pointed out the importance of combining drift-diffusion and frequency dependence analysis to reproduce experimentally observed data in PSCs. Balaguera *et al.* implemented time-dependent capacitive current equations to calculate how the PSC performance evolves with *J–V* scan frequency.[153] The capacitive behavior is governed by the geometrical capacitance as well as the movements of ions and charge carriers. The study goes beyond simple DD equations and captures kinetic processes linked to the ions and *J–V* hysteresis. As reported by Riquelme and coworkers, combining impedance spectroscopy (IS) with the DD model can reveal the underlying device physics and mechanisms responsible for recombination losses and charge collection efficiency in PSCs.[154] By investigating high-frequency impedance spectra and DD calculations, the study suggested that the steady-state performance is governed by the distribution of mobile ions within the perovskite absorber layer. Neukom *et al.*[51] presented steady-state, transient, and frequency-domain analysis of PSCs by using Setfos 4.6 from Fluxim. Using transient current analysis under dark conditions (applied voltage), the steady revealed interface recombination process modulated by the accumulation of mobile ions. The study, however, failed to explain a rise in delayed current while reversing bias (+3 V to −3 V). The study speculated mobile ion driven chemical reactions to cause the effect. Clarke *et al.*[155] implemented a time-dependent degradation factor in the recombination rate in modified DD software IonMonger. Almora *et al.*[113] proposed a short-circuit IS combined with DD modeling to investigate instability in PSCs. The study found that the ionic conduction follows different pathways at different mobile ion concentrations.

Clarke *et al.*[21] employed an approximated DD model to explain multi-feature Nyquist plots for PSCs. The model pointed out the possibility of creation of a small population of 'excess ionic defects' at DC voltage, leading to neutralization of electronic charges in the bulk perovskite layer at a different time scale than the ionic movements. The mid-frequency spectra suggested an ion-modulated recombination rate in the bulk perovskite. Both the observations are helpful in understanding the role of creation of new ionic defects and electronic–ionic interactions, which lead to *J–V* hysteresis and instability in PSCs. More of such studies at different time/frequency scales will help draw a clear picture of the underlying phenomena responsible for short- and long-term instabilities in the photovoltaic performance of PSCs.

6.3 Combining density-functional theory and DD

DD needs various input parameters to perform charge transport calculations. Some of the parameters can be obtained from experiments. However, changing the environment (*i.e.*, employing multilayers, using thin passivating layers, interface modifications, microscopic inhomogeneities, *etc.*) can alter the parameter's values while fabricating a complete device. Moreover, fabrication conditions (deposition methods, temperature, humidity and oxygen levels, post-deposition processing, storage, *etc.*) are crucial in determining the electronic, optical and optoelectronic properties of different layers. Density-functional theory (DFT) is a well-known and versatile method to calculate (but not limited to) physical, thermal, mechanical, electronic, optical and optoelectronic properties of materials.[156,157] In PSCs, DFT can help incorporating the roles of crystal structures, spin–orbit coupling, bandgap tuning by substitution/mixing, dielectric constant, photoabsorption coefficient, phonons and material stability, defect formation, ion diffusion, and surfaces and interfaces.[158] DFT has been independently used to calculate material properties,[159–161] investigating ionic defects,[159,162] and investigating interfaces and other components of PSCs.[58,90,163] Still, several phenomena taking place within a perovskite solar cell (especially at the atomistic level in ABX_3 perovskites and at the interfaces) are not very well understood and hence are not captured while simulating PSCs. Combining DFT and DD offers a way to simulate a PSC from material to device levels.[164] Marimuthu *et al.* presented a combined experimental, DFT and DD study to investigate the possibility of using dimethyl ammonium metal formate-based crystals $[(CH_3)_2NH_2]Co_{1-n}M_n(HCOO)_3$ (M = Fe, Ni and $n = 0$, 0.1) as absorbers in PSCs. DFT calculations were used to examine the structural stability, band structure, and electronic contribution of the constituent elements, and DD modeling was used to predict photovoltaic performance. The combination of DFT and DD modeling can incorporate defect formation (and hence degradation) and grain boundaries,[40] and, therefore, can predict short- and long-term performance degradation in PSCs. Overall, the integration of DFT with DD enables a multiscale simulation framework to capture both atomistic-level material properties and macroscopic device behavior, thereby enhancing the accuracy and predictive capability of perovskite solar cell simulations.

6.4 Machine learning for accelerating the calculations

Machine learning (ML) is emerging as a novel and powerful tool in materials science, thanks to its ability to (i) generate more expressive and lower dimensional representations of complex data and (ii) connect different classes of data in multimodality (*e.g.* text and images). Thus, ML models can be used to connect very different data sets and to accelerate well-established numerical models on the fly. For example, ML techniques have achieved great success in molecular dynamics[165] to accelerate numerical simulations by generating force fields on the fly or performing smart sampling of the configurational space.[166] Similarly, in the last decade, new methods based on the synergy between numerical schemes, like Dynamical Mode Decomposition (DMD) or Koopman operators,[167] have been refined and merged with data-driven methods to accelerate the simulation of partial and ordinary differential equations. All these methods are fundamentally aimed at simplifying the system, reducing its dimensionality or accelerating current numerical simulations. Moreover, ML methods can be used to generate surrogate models from simulation data, which can directly bypass the full

© 2025 The Author(s). Published by the Royal Society of Chemistry

Open Access Article. Published on 21 August 2025. Downloaded on 16.02.26 16:33:31.
This article is licensed under a Creative Commons Attribution 3.0 Unported Licence.

simulation for input–output relationships. An example of such a surrogate model is presented in ref. 168, where a Gaussian model was used to generate a surrogate model for a kinetic Monte Carlo simulation of a supercapacitor. Overall, ML is emerging as a very powerful and versatile set of tools that can work in perfect synergy with current numerical models.

6.5 Interfacing experimental data

Machine learning as a toolset has started to gain importance in the field of perovskite research and applications in analyzing and coupling experimental data. ML can be used for novel perovskite discovery, classification and characterization of samples, optimization of fabrication processes, and analysis of sample-related time series.[169] Li *et al.* have presented a method using Gaussian processes to search for high-performance cubic perovskites.[170] Behara *et al.* published an ML-based classification approach for perovskite crystal structures.[171] Characterization of samples based on Machine Vision (MV), a subset of ML with images as the main focus, has also been demonstrated to investigate film homogeneity,[172] grain characteristics[173] and some optoelectronic properties, such as bandgap and absorption behavior.[174] A promising workflow for the optimization of perovskite nanoplatelet syntheses using a mixture of ML models was reported by Lampe *et al.*[175] Time series data methods were used by Kouroudis *et al.* to predict the long-term outdoor performance of perovskite solar cells.[176] While ML as a tool in perovskite material research is still relatively new, it has already demonstrated great promise due to its flexible use cases, relatively quick deployment, and fast and fairly accurate predictions. Additionally, new methods in the field are still being developed, which may lead to the improvement of model performance in the future. The core problem hindering ML application for experimental data is the lack of available and well-curated databases. Therefore, the amount of training data is limited and very small compared to more publicly known ML models, such as large language models or image generators. To address this core issue, the scientific community should discuss what data are relevant and how best to store them, for which the FAIR principle can serve as a guideline.[177] The use of automated experimentation setups may help with the rapid production of data and may also provide opportunities to couple ML models to the setup itself, either for on-the-fly characterization or for optimization purposes.

7 Conclusions

Despite their excellent power conversion efficiency of 27%, PSCs face persistent challenges including instability, current–voltage (*J–V*) hysteresis, and interfaces and grain boundary-induced performance degradations. Drift-diffusion (DD) modeling has proven to be a powerful tool for probing the complex charge transport, recombination mechanisms and ionic defect migration in PSCs, especially where experimental techniques fall short. However, conventional DD models often rely on oversimplified assumptions and lack the fidelity to capture dynamic phenomena such as the shape and size of grains, ionic–electronic interactions, and especially the degradation of PSCs. Simplified approximations can result in misinterpretation of the calculated data despite nicely fitting with *J–V* curves. This review critically examines the evolution and limitations of DD modeling in PSCs, highlighting key areas where accuracy and predictive power can be improved. We explore strategies for incorporating sub-models for traps, recombination, grain boundaries, mobility, ionic–electronic interactions, photon recycling, and quantum effects. We also emphasize on the importance of integrating experimental data to minimize approximations. The possibility of including degradation pathways and time/frequency domain analysis has been discussed to gain insight into instability. For modeling parameters not directly accessible through experiments, the synergy between DD and Density Functional Theory is discussed as a pathway to bridge atomistic and device-level simulations. Furthermore, the possibility of combining machine learning and interfacing experimental data has been presented to speed up the simulations and improve robustness and reliability. By mapping the evolution of DD modeling and identifying key areas for refinement, this work provides a foundation for future efforts to develop predictive, high-fidelity simulation tools for perovskite photovoltaics.

Author contributions

Both authors contributed to the conceptualization, literature review, manuscript writing, review and editing parts of the paper.

Conflicts of interest

There are no conflicts to declare.

Data availability

No primary research results, software, or code have been included and no new data were generated or analyzed as part of this review.

Acknowledgements

This work was financially supported by the Indian Institute of Technology Guwahati *via* grant no. SESESUGIITG01472AJSN001.

Notes and references

1 D. A. Egger, A. Bera, D. Cahen, G. Hodes, T. Kirchartz, L. Kronik, R. Lovrincic, A. M. Rappe, D. R. Reichman and O. Yaffe, *Adv. Mater.*, 2018, **30**, 1800691.
2 M. B. Johnston and L. M. Herz, *Acc. Chem. Res.*, 2016, **49**, 146–154.
3 J. S. Manser, J. A. Christians and P. V. Kamat, *Chem. Rev.*, 2016, **116**, 12956–13008.
4 NREL, *Best Research-Cell Efficiency Chart*, 2025, **https://www.nrel.gov/pv/cell-efficiency**, accessed on 01 Aug 2025.

Open Access Article. Published on 21 August 2025. Downloaded on 16.02.26 16:33:31.
This article is licensed under a Creative Commons Attribution 3.0 Unported Licence.

5 Y. Zhou, L. M. Herz, A. K. Jen and M. Saliba, *Nat. Energy*, 2022, **7**, 794–807.
6 T. S. Sherkar, C. Momblona, L. Gil-Escrig, H. J. Bolink and L. J. A. Koster, *Adv. Energy Mater.*, 2017, **7**, 1602432.
7 A. Sengupta, M. A. Afroz, B. Sharma, S. Choudhary, N. Pant, Y. Gulia, N. Pai, D. Angmo and S. Satapathi, *Sustainable Energy Fuels*, 2025, **9**, 3999–4022.
8 M. I. H. Ansari, A. Qurashi and M. K. Nazeeruddin, *J. Photochem. Photobiol., C*, 2018, **35**, 1–24.
9 B. Conings, J. Drijkoningen, N. Gauquelin, A. Babayigit, J. D'Haen, L. D'Olieslaeger, A. Ethirajan, J. Verbeeck, J. Manca, E. Mosconi, F. De Angelis and H.-G. Boyen, *Adv. Energy Mater.*, 2015, **5**, 1500477.
10 E. H. Balaguera and J. Bisquert, *ACS Energy Lett.*, 2024, **9**, 478–486.
11 S. Tammireddy, M. N. Lintangpradipto, O. Telschow, M. H. Futscher, B. Ehrler, O. M. Bakr, Y. Vaynzof and C. Deibel, *J. Phys. Chem. Lett.*, 2024, **15**, 1363–1372.
12 W. Peng, C. Aranda, O. M. Bakr, G. Garcia-Belmonte, J. Bisquert and A. Guerrero, *ACS Energy Lett.*, 2018, **3**, 1477–1481.
13 S. Reichert, Q. An, Y.-W. Woo, A. Walsh, Y. Vaynzof and C. Deibel, *Nat. Commun.*, 2020, **11**, 6098.
14 C. Li, A. Guerrero, Y. Zhong, A. Gräser, C. A. M. Luna, J. Köhler, J. Bisquert, R. Hildner and S. Huettner, *Small*, 2017, **13**, 1701711.
15 G. De Moor, N. Charvin, C. Farha, T. Meyer, L. Perrin, E. Planes and L. Flandin, *Sol. RRL*, 2024, **8**, 2300998.
16 A. Singh and A. Gagliardi, *2020 IEEE 20th International Conference on Nanotechnology (IEEE-NANO)*, 2020, pp. 227–232.
17 G. Richardson, S. E. O'Kane, R. G. Niemann, T. A. Peltola, J. M. Foster, P. J. Cameron and A. B. Walker, *Energy Environ. Sci.*, 2016, **9**, 1476–1485.
18 Z. S. Wang, Y. An, X. Ren, H. Zhang, Z. Huang, H.-L. Yip, Z. Huang and W. C. H. Choy, *Nat. Commun.*, 2024, **15**, 9647.
19 H. Baishya, R. D. Adhikari, M. J. Patel, D. Yadav, T. Sarmah, M. Alam, M. Kalita and P. K. Iyer, *J. Energy Chem.*, 2024, **94**, 217–253.
20 Y. Cui, C. Chen, C. Li, L. Chen, S. S. Bista, X. Liu, Y. Li, R. A. Awni, Z. Song and Y. Yan, *ACS Appl. Mater. Interfaces*, 2020, **12**, 10588–10596.
21 W. Clarke, G. Richardson and P. Cameron, *Adv. Energy Mater.*, 2024, 2400955.
22 L. Xu, R. Molaei Imenabadi, W. G. Vandenberghe and J. W. P. Hsu, *APL Mater.*, 2018, **6**, 036104.
23 P. Caprioglio, C. M. Wolff, O. J. Sandberg, A. Armin, B. Rech, S. Albrecht, D. Neher and M. Stolterfoht, *Adv. Energy Mater.*, 2020, **10**, 2000502.
24 A. Singh and A. Gagliardi, *EPJ Photovoltaics*, 2021, **12**, 4.
25 K. T. Tanko, S. R. Raga, N. Vahedigharehchopogh, F. Baumann, M. Karimipour, R. A. Miranda-Gamboa and M. Lira-Cantú, *Sol. RRL*, 2025, 202500162.
26 T. Y. Ahmed, D. A. Noori, K. K. Ahmed and S. B. Aziz, *Mater. Sci. Semicond. Process.*, 2024, **178**, 108459.
27 B. Olyaeefar, S. Ahmadi-Kandjani and A. Asgari, *Sol. Energy Mater. Sol. Cells*, 2018, **180**, 76–82.
28 P. Saxena and N. E. Gorji, *IEEE J. Photovoltaics*, 2019, **9**, 1693–1698.
29 A. Singh, F. Matteocci, H. Zhu, D. Rossi, S. Mejaouri, S. Cacovich, M. auf Der Maur, F. Sauvage, A. Gagliardi, M. Graetzel, *et al.*, *Sol. RRL*, 2021, **5**, 2100277.
30 N. Rodkey, I. Gomar-Fernández, F. Ventosinos, C. Roldan-Carmona, L. J. A. Koster and H. J. Bolink, *ACS Energy Lett.*, 2024, **9**, 927–933.
31 M. Singh, R. Kumar, V. Singh, *et al.*, *Mater. Res. Express*, 2019, **6**, 115611.
32 T.-Y. Huang, C.-C. Li, Y.-H. Lai, X.-K. Gao, Y.-C. Huang, C.-C. Yang, T.-L. Wu and C.-S. Tan, *Sol. RRL*, 2025, **9**, 2500181.
33 M. Kerara, A. Naas, A. Gueddim and O. Meglali, *Transactions on Electrical and Electronic Materials*, 2024, **25**, 665–673.
34 P. Calado, I. Gelmetti, B. Hilton, M. Azzouzi, J. Nelson and P. R. Barnes, *J. Comput. Electron.*, 2022, **21**, 960–991.
35 N. E. Courtier, J. M. Cave, A. B. Walker, G. Richardson and J. M. Foster, *J. Comput. Electron.*, 2019, **18**, 1435–1449.
36 V. M. Le Corre, M. Stolterfoht, L. Perdigon Toro, M. Feuerstein, C. Wolff, L. Gil-Escrig, H. J. Bolink, D. Neher and L. J. A. Koster, *ACS Appl. Energy Mater.*, 2019, **2**, 6280–6287.
37 A. Singh, W. Kaiser and A. Gagliardi, *Sol. Energy Mater. Sol. Cells*, 2021, **221**, 110912.
38 R. Zhou, Y. Chen, L. Zhou, Y. Yao, Y. Liu, C. Wang, L. Niu and L. Chen, *Sol. Energy Mater. Sol. Cells*, 2024, **264**, 112616.
39 T. S. Sherkar, C. Momblona, L. Gil-Escrig, J. Ávila, M. Sessolo, H. J. Bolink and L. J. A. Koster, *ACS Energy Lett.*, 2017, **2**, 1214–1222.
40 W. Kaiser, K. Hussain, A. Singh, A. A. Alothman, D. Meggiolaro, A. Gagliardi, E. Mosconi and F. De Angelis, *J. Mater. Chem. A*, 2022, **10**, 24854–24865.
41 J. Zhang, S. Tang, M. Zhu, Z. Li, Z. Cheng, S. Xiang and Z. Zhang, *Energy Environ. Mater.*, 2024, e12696.
42 A.-F. Castro-Méndez, J. Hidalgo and J.-P. Correa-Baena, *Adv. Energy Mater.*, 2019, **9**, 1901489.
43 S. Jariwala, H. Sun, G. W. Adhyaksa, A. Lof, L. A. Muscarella, B. Ehrler, E. C. Garnett and D. S. Ginger, *Joule*, 2019, **3**, 3048–3060.
44 T. Zhang, H. Luo, M. Abdi-Jalebi, H. Chen and L. Zuo, *Information & Functional Materials*, 2024, **1**, 87–107.
45 A. Pecchia, D. Gentilini, D. Rossi, M. Auf der Maur and A. Di Carlo, *Nano Lett.*, 2016, **16**, 988–992.
46 D. Rossi, A. Pecchia, M. A. der Maur, T. Leonhard, H. Röhm, M. J. Hoffmann, A. Colsmann and A. D. Carlo, *Nano Energy*, 2018, **48**, 20–26.
47 D. Rossi, M. A. der Maur, A. Pecchia and A. Di Carlo, *2017 International Conference on Numerical Simulation of Optoelectronic Devices (NUSOD)*, 2017, pp. 21–22.
48 M. I. Hossain, A. M. Saleque, S. Ahmed, I. Saidjafarzoda, M. Shahiduzzaman, W. Qarony, D. Knipp, N. Biyikli and Y. H. Tsang, *Nano Energy*, 2021, **79**, 105400.
49 C. Gao, D. Du and W. Shen, *Carbon Neutrality*, 2022, **1**, 9.
50 K. Hussain and A. Gagliardi, *Sol. Energy*, 2022, **243**, 193–202.

© 2025 The Author(s). Published by the Royal Society of Chemistry

Open Access Article. Published on 21 August 2025. Downloaded on 16.02.26 16:33:31.
This article is licensed under a Creative Commons Attribution 3.0 Unported Licence.

51 M. T. Neukom, A. Schiller, S. Züfle, E. Knapp, J. Ávila, D. Pérez-del Rey, C. Dreessen, K. P. Zanoni, M. Sessolo, H. J. Bolink, *et al.*, *ACS Appl. Mater. Interfaces*, 2019, **11**, 23320–23328.
52 P. Calado, A. M. Telford, D. Bryant, X. Li, J. Nelson, B. C. O'Regan and P. R. Barnes, *Nat. Commun.*, 2016, **7**, 13831.
53 W. Shockley and W. Read Jr, *Phys. Rev.*, 1952, **87**, 835.
54 R. Hall, *Phys. Rev.*, 1951, **83**, 228.
55 J. I. Pankove, *Optical Processes in Semiconductors*, Courier Corporation, 1975.
56 J. M. Ball, S. D. Stranks, M. T. Hörantner, S. Hüttner, W. Zhang, E. J. Crossland, I. Ramirez, M. Riede, M. B. Johnston, R. H. Friend and H. J. Snaith, *Energy Environ. Sci.*, 2015, **8**, 602–609.
57 N. Tessler and Y. Vaynzof, *ACS Energy Lett.*, 2020, **5**, 1260–1270.
58 L. Canil, T. Cramer, B. Fraboni, D. Ricciarelli, D. Meggiolaro, *et al.*, *Energy Environ. Sci.*, 2021, **14**, 1429–1438.
59 P. Calado and P. R. Barnes, *Nat. Energy*, 2021, **6**, 589–591.
60 L. Lei, S. Zhang, S. Yang, X. Li, Y. Yu, Q. Wei, Z. Ni and M. Li, *Nanotechnology*, 2018, **29**, 255201.
61 R. Alkarsifi, J. Ackermann and O. Margeat, *J. Met., Mater. Miner.*, 2022, **32**, 1–22.
62 Q. An, F. Paulus, D. Becker-Koch, C. Cho, Q. Sun, A. Weu, S. Bitton, N. Tessler and Y. Vaynzof, *Matter*, 2021, **4**, 1683–1701.
63 J. Xing, Q. Wang, Q. Dong, Y. Yuan, Y. Fang and J. Huang, *Phys. Chem. Chem. Phys.*, 2016, **18**, 30484–30490.
64 Y. Shao, Y. Fang, T. Li, Q. Wang, Q. Dong, Y. Deng, Y. Yuan, H. Wei, M. Wang, A. Gruverman, *et al.*, *Energy Environ. Sci.*, 2016, **9**, 1752–1759.
65 B. Roose, A. Ummadisingu, J.-P. Correa-Baena, M. Saliba, A. Hagfeldt, M. Graetzel, U. Steiner and A. Abate, *Nano Energy*, 2017, **39**, 24–29.
66 S. Iftiquar and J. Yi, *Mater. Sci. Semicond. Process.*, 2018, **79**, 46–52.
67 V. Nandal and P. R. Nair, *J. Appl. Phys.*, 2019, **125**, 173110.
68 W. Yao, S. Fang, Z. Hu, L. Huang, X. Liu, H. Zhang, J. Zhang and Y. Zhu, *Small*, 2022, **18**, 2105140.
69 P. Jia, L. Qin, D. Zhao, Y. Tang, B. Song, J. Guo, X. Li, L. Li, Q. Cui, Y. Hu, *et al.*, *Adv. Funct. Mater.*, 2021, **31**, 2107125.
70 Z. Chu, M. Yang, P. Schulz, D. Wu, X. Ma, E. Seifert, L. Sun, X. Li, K. Zhu and K. Lai, *Nat. Commun.*, 2017, **8**, 1–8.
71 P. You, G. Tang, J. Cao, D. Shen, T.-W. Ng, Z. Hawash, N. Wang, C.-K. Liu, W. Lu, Q. Tai, *et al.*, *Light: Sci. Appl.*, 2021, **10**, 68.
72 A. Hajjiah, *Opt. Quantum Electron.*, 2025, **57**, 215.
73 M. Liu, M. Endo, A. Shimazaki, A. Wakamiya and Y. Tachibana, *ACS Appl. Energy Mater.*, 2018, **1**, 3722–3732.
74 D. Ramirez, K. Schutt, J. F. Montoya, S. Mesa, J. Lim, H. J. Snaith and F. Jaramillo, *J. Phys. Chem. C*, 2018, **122**, 21239–21247.
75 M. H. Mohammadi, M. Eskandari and D. Fathi, *Sci. Rep.*, 2023, **13**, 18584.
76 E. Ouabida, M. Kibbou, Z. Haman and A. Ainane, *Mater. Today Commun.*, 2023, **35**, 106354.
77 S. Haque, M. Alexandre, C. Baretzky, D. Rossi, F. De Rossi, A. T. Vicente, F. Brunetti, H. Águas, R. A. Ferreira, E. Fortunato, *et al.*, *ACS Photonics*, 2022, **9**, 2408–2421.
78 F. Jahantigh and S. Bagher Ghorashi, *Nano*, 2019, **14**, 1950127.
79 X. Sun, R. Asadpour, W. Nie, A. D. Mohite and M. A. Alam, *IEEE J. Photovoltaics*, 2015, **5**, 1389–1394.
80 P. K. Patel, *Sci. Rep.*, 2021, **11**, 3082.
81 A. Singh and A. Gagliardi, *Sol. Energy*, 2019, **187**, 39–46.
82 S. Gohri, J. Madan and R. Pandey, *J. Electron. Mater.*, 2024, 1–9.
83 A. Kumar, P. Sharma, *et al.*, *Sol. Energy*, 2023, **259**, 63–71.
84 J. B. Patel, A. D. Wright, K. B. Lohmann, K. Peng, C. Q. Xia, J. M. Ball, N. K. Noel, T. W. Crothers, J. Wong-Leung, H. J. Snaith, *et al.*, *Adv. Energy Mater.*, 2020, **10**, 1903653.
85 H. Bencherif and M. K. Hossain, *Sol. Energy*, 2022, **248**, 137–148.
86 V. Campanari, F. Martelli, A. Agresti, S. Pescetelli, N. Y. Nia, F. Di Giacomo, D. Catone, P. O'Keeffe, S. Turchini, B. Yang, J. Suo, A. Hagfeldt and A. Di Carlo, *Sol. RRL*, 2022, **6**, 2200049.
87 H. Phirke, S. Gharabeiki, A. Singh, A. Krishna, S. Siebentritt and A. Redinger, *APL Energy*, 2024, **2**, 016111.
88 R. García-Rodríguez, A. J. Riquelme, M. Cowley, K. Valadez-Villalobos, G. Oskam, L. J. Bennett, M. J. Wolf, L. Contreras-Bernal, P. J. Cameron, A. B. Walker, *et al.*, *Energy Technol.*, 2022, **10**, 2200507.
89 C. M. Wolff, P. Caprioglio, M. Stolterfoht and D. Neher, *Adv. Mater.*, 2019, **31**, 1902762.
90 A. Krishna, V. Skorjanc, M. Dankl, J. Hieulle, H. Phirke, A. Singh, E. A. Alharbi, H. Zhang, F. Eickemeyer, S. M. Zakeeruddin, *et al.*, *ACS Energy Lett.*, 2023, **8**, 3604–3613.
91 L. Wagner, P. Schygulla, J. P. Herterich, M. Elshamy, D. Bogachuk, S. Zouhair, S. Mastroianni, U. Würfel, Y. Liu, S. M. Zakeeruddin, M. Grätzel, A. Hinsch and S. W. Glunz, *Matter*, 2022, **5**, 2352–2364.
92 J. Xia, C. Liang, H. Gu, S. Mei, S. Li, N. Zhang, S. Chen, Y. Cai and G. Xing, *Energy Environ. Mater.*, 2023, **6**, e12296.
93 T. Yang, W. Zhao, X. Liu and S. Liu, *Adv. Energy Mater.*, 2023, **13**, 2204192.
94 S. Wang, H. Guo and Y. Wu, *Mater. Futures*, 2023, **2**, 012105.
95 C. Chen, S. Zhang, S. Wu, W. Zhang, H. Zhu, Z. Xiong, Y. Zhang and W. Chen, *RSC Adv.*, 2017, **7**, 35819–35826.
96 N. Shibayama, H. Kanda, T. W. Kim, H. Segawa and S. Ito, *APL Mater.*, 2019, **7**, 031117.
97 S. Bitton and N. Tessler, *J. Mater. Chem. C*, 2021, **9**, 1888–1894.
98 L. Tian, W. E. Sha, H. Xie, D. Liu, T.-G. Sun, Y.-S. Xia and W. Chen, *J. Appl. Phys.*, 2024, **135**, 225703.
99 W. Zhu, S. Wang, X. Zhang, A. Wang, C. Wu and F. Hao, *Small*, 2022, **18**, 2105783.
100 G. Nagabhushana, R. Shivaramaiah and A. Navrotsky, *Proc. Natl. Acad. Sci. U. S. A.*, 2016, **113**, 7717–7721.

Open Access Article. Published on 21 August 2025. Downloaded on 16.02.26 16:33:31.
This article is licensed under a Creative Commons Attribution 3.0 Unported Licence.

101 W.-J. Yin, T. Shi and Y. Yan, *Appl. Phys. Lett.*, 2014, **104**, 063903.
102 S. Srivastava, S. Ranjan, L. Yadav, T. Sharma, S. Choudhary, D. Agarwal, A. Singh, S. Satapathi, R. K. Gupta, A. Garg, *et al.*, *Commun. Mater.*, 2023, **4**, 52.
103 D. Moia and J. Maier, *ACS Energy Lett.*, 2021, **6**, 1566–1576.
104 S. Reichert, J. Flemming, Q. An, Y. Vaynzof, J.-F. Pietschmann and C. Deibel, *Phys. Rev. Appl.*, 2020, **13**, 034018.
105 Q. Wali, M. Aamir, A. Ullah, F. J. Iftikhar, M. E. Khan, J. Akhtar and S. Yang, *Chem. Rec.*, 2022, **22**, e202100150.
106 P. Lopez-Varo, J. A. Jimenez-Tejada, M. Garcia-Rosell, J. A. Anta, S. Ravishankar, A. Bou and J. Bisquert, *ACS Energy Lett.*, 2017, **2**, 1450–1453.
107 S. Bitton and N. Tessler, *Energy Environ. Sci.*, 2023, **16**, 2621–2628.
108 A. Schiller, S. Jenatsch, B. Blülle, M. A. Torre Cachafeiro, F. Ebadi, N. Kabir, M. Othman, C. M. Wolff, A. Hessler-Wyser, C. Ballif, *et al.*, *J. Phys. Chem. Lett.*, 2024, **15**, 11252–11258.
109 M. Minbashi and E. Yazdani, *Sci. Rep.*, 2022, **12**, 14916.
110 A. Gagliardi and A. Abate, *ACS Energy Lett.*, 2017, **3**, 163–169.
111 S. van Reenen, M. Kemerink and H. J. Snaith, *J. Phys. Chem. Lett.*, 2015, **6**, 3808–3814.
112 K. Domanski, B. Roose, T. Matsui, M. Saliba, S.-H. Turren-Cruz, J.-P. Correa-Baena, C. R. Carmona, G. Richardson, J. M. Foster, F. De Angelis, J. M. Ball, A. Petrozza, N. Mine, M. K. Nazeeruddin, W. Tress, M. Grätzel, U. Steiner, A. Hagfeldt and A. Abate, *Energy Environ. Sci.*, 2017, **10**, 604–613.
113 O. Almora, P. López-Varo, R. Escalante, J. Mohanraj, L. F. Marsal, S. Olthof and J. A. Anta, *J. Appl. Phys.*, 2024, **136**, 094502.
114 W. Zhang, V. M. Burlakov, D. J. Graham, T. Leijtens, A. Osherov, V. Bulović, H. J. Snaith, D. S. Ginger, S. D. Stranks, *et al.*, *Nat. Commun.*, 2016, **7**, 11683.
115 T. Leijtens, S. D. Stranks, G. E. Eperon, R. Lindblad, E. M. Johansson, I. J. McPherson, H. Rensmo, J. M. Ball, M. M. Lee and H. J. Snaith, *ACS Nano*, 2014, **8**, 7147–7155.
116 S. Shao, M. Abdu-Aguye, T. S. Sherkar, H.-H. Fang, S. Adjokatse, G. t. Brink, B. J. Kooi, L. J. A. Koster and M. A. Loi, *Adv. Funct. Mater.*, 2016, **26**, 8094–8102.
117 J. Euvrard, Y. Yan and D. B. Mitzi, *Nat. Rev. Mater.*, 2021, **6**, 531–549.
118 L. M. Herz, *ACS Energy Lett.*, 2017, **2**, 1539–1548.
119 C. Motta, F. El-Mellouhi and S. Sanvito, *Sci. Rep.*, 2015, **5**, 12746.
120 O. G. Reid, M. Yang, N. Kopidakis, K. Zhu and G. Rumbles, *ACS Energy Lett.*, 2016, **1**, 561–565.
121 S.-J. Yoo and J.-J. Kim, *Macromol. Rapid Commun.*, 2015, **36**, 984–1000.
122 M. Cardona and Y. Y. Peter, *Fundamentals of Semiconductors*, Springer, 3rd edn, 2007.
123 D. A. Neamen, *Semiconductor Physics and Devices*, McGraw-Hill, 2011.
124 A. Biewald, N. Giesbrecht, T. Bein, P. Docampo, A. Hartschuh and R. Ciesielski, *ACS Appl. Mater. Interfaces*, 2019, **11**, 20838–20844.
125 M. Z. Mayers, L. Z. Tan, D. A. Egger, A. M. Rappe and D. R. Reichman, *Nano Lett.*, 2018, **18**, 8041–8046.
126 T. J. Savenije, C. S. Ponseca Jr, L. Kunneman, M. Abdellah, K. Zheng, Y. Tian, Q. Zhu, S. E. Canton, I. G. Scheblykin, T. Pullerits, *et al.*, *J. Phys. Chem. Lett.*, 2014, **5**, 2189–2194.
127 K. Anoop and T. Ahipa, *Sol. Energy*, 2023, **263**, 111937.
128 A. Raj, M. Kumar and A. Anshul, *Mater. Today Chem.*, 2021, **22**, 100595.
129 G. Ren, W. Han, Y. Deng, W. Wu, Z. Li, J. Guo, H. Bao, C. Liu and W. Guo, *J. Mater. Chem. A*, 2021, **9**, 4589–4625.
130 Y. Xu, Y. Li, S. Li, F. Balestra, G. Ghibaudo, W. Li, Y.-F. Lin, H. Sun, J. Wan, X. Wang, *et al.*, *Adv. Funct. Mater.*, 2020, **30**, 1904508.
131 Z. Bin, Z. Liu, Y. Qiu and L. Duan, *Adv. Opt. Mater.*, 2018, **6**, 1800536.
132 A. Mityashin, D. Cheyns, B. P. Rand and P. Heremans, *Appl. Phys. Lett.*, 2012, **100**, 053305.
133 V. Arkhipov, E. Emelianova, P. Heremans and H. Bässler, *Phys. Rev. B:Condens. Matter Mater. Phys.*, 2005, **72**, 235202.
134 V. Arkhipov, P. Heremans, E. Emelianova and H. Baessler, *Phys. Rev. B:Condens. Matter Mater. Phys.*, 2005, **71**, 045214.
135 M. Koopmans, M. A. Leiviskä, J. Liu, J. Dong, L. Qiu, J. C. Hummelen, G. Portale, M. C. Heiber and L. J. A. Koster, *ACS Appl. Mater. Interfaces*, 2020, **12**, 56222–56230.
136 G. Masetti, M. Severi and S. Solmi, *IEEE Trans. Electron Devices*, 1983, **30**, 764–769.
137 C. Lombardi, S. Manzini, A. Saporito and M. Vanzi, *IEEE Trans. Comput. Aided Des. Integrated Circ. Syst.*, 1988, **7**, 1164–1171.
138 B. Maynard, Q. Long, E. A. Schiff, M. Yang, K. Zhu, R. Kottokkaran, H. Abbas and V. L. Dalal, *Appl. Phys. Lett.*, 2016, **108**, 173505.
139 N. K. Elangovan, R. Kannadasan, B. Beenarani, M. H. Alsharif, M.-K. Kim and Z. H. Inamul, *Energy Rep.*, 2024, **11**, 1171–1190.
140 N. Ahn and M. Choi, *Adv. Sci.*, 2024, **11**, 2306110.
141 S. Macpherson, T. A. Doherty, A. J. Winchester, S. Kosar, D. N. Johnstone, Y.-H. Chiang, K. Galkowski, M. Anaya, K. Frohna, A. N. Iqbal, *et al.*, *Nature*, 2022, **607**, 294–300.
142 V. Nandal and P. R. Nair, *ACS Nano*, 2017, **11**, 11505–11512.
143 J. A. McLeod and L. Liu, *J. Phys. Chem. Lett.*, 2018, **9**, 2411–2417.
144 L. Lanzetta, T. Webb, N. Zibouche, X. Liang, D. Ding, G. Min, R. J. Westbrook, B. Gaggio, T. J. Macdonald, M. S. Islam, *et al.*, *Nat. Commun.*, 2021, **12**, 1–11.
145 S. Kundu and T. L. Kelly, *EcoMat*, 2020, **2**, e12025.
146 F. Sacconi, M. A. der Maur, M. Povolotskyi, G. Romano, A. Pecchia, G. Penazzi, S. Bellocchio and A. Di Carlo, *TIBERCAD User Manual*, 2009.
147 Y. P. Varshni, *Physica*, 1967, **34**, 149–154.
148 M. P. Lumb, M. A. Steiner, J. F. Geisz and R. J. Walters, *J. Appl. Phys.*, 2014, **116**, 194504.

© 2025 The Author(s). Published by the Royal Society of Chemistry

Open Access Article. Published on 21 August 2025. Downloaded on 16.02.26 16:33:31.
This article is licensed under a Creative Commons Attribution 3.0 Unported Licence.

149 U. Aeberhard, S. Zeder and B. Ruhstaller, *Sol. RRL*, 2024, **8**, 2400264.
150 S. Zeder, B. Ruhstaller and U. Aeberhard, *Phys. Rev. Appl.*, 2022, **17**, 014023.
151 R. Brenes, M. Laitz, J. Jean, D. W. deQuilettes and V. Bulović, *Phys. Rev. Appl.*, 2019, **12**, 014017.
152 A. Bou, H. Abolins, A. Ashoka, H. Cruanyes, A. Guerrero, F. Deschler and J. Bisquert, *ACS Energy Lett.*, 2021, **6**, 2248–2255.
153 E. H. Balaguera and J. Bisquert, *Energy Fuels*, 2025, **3**, 3638–3648.
154 A. Riquelme, L. J. Bennett, N. E. Courtier, M. J. Wolf, L. Contreras-Bernal, A. B. Walker, G. Richardson and J. A. Anta, *Nanoscale*, 2020, **12**, 17385–17398.
155 W. Clarke, P. Cameron and G. Richardson, *J. Phys. Chem. Lett.*, 2024, **15**, 11730–11736.
156 W. Koch and M. C. Holthausen, *A Chemist's Guide to Density Functional Theory*, John Wiley & Sons, 2nd edn, 2015.
157 F. Giustino, *Materials Modelling Using Density Functional Theory: Properties and Predictions*, Oxford University Press, 2014.
158 C.-J. Yu, *J. Phys.: Energy*, 2019, **1**, 022001.
159 W.-J. Yin, T. Shi and Y. Yan, *Adv. Mater.*, 2014, **26**, 4653–4658.
160 X. Diao, Y. Diao, Y. Tang, G. Zhao, Q. Gu, Y. Xie, Y. Shi, P. Zhu and L. Zhang, *Sci. Rep.*, 2022, **12**, 12633.
161 R. K. Pingak, A. Harbi, M. Moutaabbid, A. Z. Johannes, N. U. J. Hauwali, M. Bukit, F. Nitti and M. Z. Ndii, *Mater. Res. Express*, 2023, **10**, 095507.
162 D. Meggiolaro and F. De Angelis, *ACS Energy Lett.*, 2018, **3**, 2206–2222.
163 K. D. Jayan and V. Sebastian, *AIP Conf. Proc.*, 2019, 020036.
164 S. Marimuthu, S. Pandiaraj, M. Muthuramamoorthy, K. E. Alzahrani, A. N. Alodhayb, S. Pitchaimuthu and A. N. Grace, *Phys. Chem. Chem. Phys.*, 2024, **26**, 4262–4277.
165 S. Batzner, A. Musaelian, L. Sun, M. Geiger, J. P. Mailoa, M. Kornbluth, N. Molinari, T. E. Smidt and B. Kozinsky, *Nat. Commun.*, 2022, **13**, 2453.
166 G. A. Siddiqui, J. A. Stebani, D. Wragg, P.-S. Koutsourelakis, A. Casini and A. Gagliardi, *Chem.–Eur. J.*, 2023, **29**, e202302375.
167 H. Arbabi and I. Mezic, *SIAM J. Appl. Dyn. Syst.*, 2017, **16**, 2096–2126.
168 I. Kouroudis, M. Gößwein and A. Gagliardi, *J. Phys. Chem. A*, 2023, **127**, 5967–5978.
169 F. Mayr, M. Harth, I. Kouroudis, M. Rinderle and A. Gagliardi, *J. Phys. Chem. Lett.*, 2022, **13**, 1940–1951.
170 Z. Li, L. E. Achenie and H. Xin, *ACS Catal.*, 2020, **10**, 4377–4384.
171 S. Behara, T. Poonawala and T. Thomas, *Comput. Mater. Sci.*, 2021, **188**, 110191.
172 N. Taherimakhsousi, B. P. MacLeod, F. G. Parlane, T. D. Morrissey, E. P. Booker, K. E. Dettelbach and C. P. Berlinguette, *npj Comput. Mater.*, 2020, **6**, 111.
173 Y. Zhang and Y. Zhou, *Acc. Mater. Res.*, 2023, **4**, 209–211.
174 Y. Liu, W. Yan, H. Zhu, Y. Tu, L. Guan and X. Tan, *Org. Electron.*, 2022, **101**, 106426.
175 C. Lampe, I. Kouroudis, M. Harth, S. Martin, A. Gagliardi and A. S. Urban, *Adv. Mater.*, 2023, **35**, 2208772.
176 I. Kouroudis, K. T. Tanko, M. Karimipour, A. B. Ali, D. K. Kumar, V. Sudhakar, R. K. Gupta, I. Visoly-Fisher, M. Lira-Cantu and A. Gagliardi, *ACS Energy Lett.*, 2024, **9**, 1581–1586.
177 T. J. Jacobsson, A. Hultqvist, A. García-Fernández, A. Anand, A. Al-Ashouri, A. Hagfeldt, A. Crovetto, A. Abate, A. G. Ricciardulli, A. Vijayan, *et al.*, *Nat. Energy*, 2022, **7**, 107–115.

© 2025 The Author(s). Published by the Royal Society of Chemistry